DEPARTMENT OF PHYSICS
UNIVERSITY OF JYVÄSKYLÄ
RESEARCH REPORT No. 7/2016

INTERACTION BETWEEN SURFACE PLASMON POLARITONS AND MOLECULES IN STRONG COUPLING LIMIT

BY
SVITLANA BAIEVA

Academic Dissertation
for the Degree of
Doctor of Philosophy

To be presented, by permission of the
Faculty of Mathematics and Science
of the University of Jyväskylä,
for public examination in Auditorium FYS-1 of the
University of Jyväskylä on June 30, 2016
at 12 o'clock

Jyväskylä, Finland
June 2016

Preface

The work reviewed in this thesis has been carried out during the years 2011-2016 at the Department of Physics at the University of Jyväskylä in Nanoscience Center.

First of all I would like to thank my supervisor Dr. Jussi Toppari for the guidance and support during my studies. The work in his group gave me opportunity to collaborate with many brilliant people. I am grateful to all former and present members of our group. I wish to thank Dr. Tommi Hakala who introduced me the fascinating field of plasmonics. Particularly I wish to thank Dr. Heli Lehtivuori, Dr. Janne Simonen, Mr. Tommi Isoniemi, Mr. Boxuan Shen and Mr. Kosti Tapio.

I wish to express my gratitude to Prof. Janne Ihalainen, Prof. Tero Heikkilä and Dr. Gerrit Groenhof for collaboration.

In addition I would like to thank for the essential technical support laboratory engineers of Nanoscience center Dr. Pasi Myllyperkiö, Dr. Kimmo Kinnunen and Mr. Tarmo Suppula. I am grateful to office personnel of the Department of Physics and the Nanoscience center.

At last, I want to thank Andrii Torgovkin, my family and my friends for their support and patience.

Financial support from Academy of Finland is gratefully acknowledged.

Jyväskylä, April 2016

Svitlana Baieva

Abstract

Baieva, Svitlana
Interaction between surface plasmon polaritons and molecules in strong coupling limit
Jyväskylä : University of Jyväskylä , 2016, 78 p.
(Research report/Department of Physics, University of Jyväskylä ,
ISSN 0075-465X; 7/2016)
ISBN 978-951-39-6676-8 PDF 978-951-39-6677-5
diss.

Miniaturization of optical elements and their integration to electronic circuits is limited by diffraction limit. It was realized that light being coupled to surface plasmons (SP) can overcome this limit. Employing also optically active molecules in combination with SPs can drive optical circuits to nm-scale and add functionalities. For efficient performance of plasmonic elements involving fluorescent dye molecules investigation of physics behind their interaction is of high priority. In this thesis interaction between surface plasmon polaritons (SPPs) and different dye molecules has been studied, especially within strong coupling limit, which brings in totally new physical properties in the form of hybrid SP-molecule polariton states.

Strong coupling with SPPs was achieved altogether for Sulforhodamine 101 (SR101), Rhodamine 6G (R6G), TDBC and β-carotene molecules. The measurements were done in Kretschmann geometry using two complementary detection techniques. In attenuated total internal reflection (ATR) experiments the signature of strong coupling, *i.e.*, energy splittings in dispersion curve, was observed for samples having sufficient amount of molecules. The value of energy splitting is directly proportional to the square root of total molecular absorption, which is analogous to the strong coupling of dyes with photons inside optical microcavities. Collected scattered radiation also shows features of strong coupling. Moreover the energy gaps values are increased indicating role of interaction time.

We performed also molecule excitation directly by laser in reverse Kretschmann configuration and analyzed the emission patterns revealing clear surface plasmon coupled fluorescence of β-carotene. By increasing the concentration of β-carotene

we were able to collect also surface plasmon coupled Raman scattering signal.

Light scattered out due to surface roughness during the SPP propagation is always p (TM)-polarized when detected on the direction perpendicular to the surface of silver film. However, we observe polarization conversion of scattered SPP-molecule polariton in the case of R6G and TDBC dyes. We assign this rather to the properties of strongly coupled molecular state then to conversion due to surface plasmon polariton scattering on metallic film imperfections. By comparing results of different dyes we can conclude that higher Stokes shift, leading to the faster decay of the absorption state of the molecule, results in the loss of the polarization conversion returning thus the pure SPP scattering behavior.

Keywords surface plasmon polariton, dye molecules, strong coupling, surface plasmon coupled emission, scattering

Author's address Svitlana Baieva
Department of Physics
University of Jyväskylä
Finland

Supervisor Doctor Jussi Toppari
Department of Physics
University of Jyväskylä
Finland

Reviewers Doctor Johannes Feist
Departamento de Física Teórica de la Materia Condensada
Universidad Autónoma de Madrid
Spain

Doctor Tal Schwartz
School of Chemistry
Tel Aviv University
Israel

Opponent Professor Bill Barnes
School of Physics and Astronomy
University of Exeter
UK

List of Abbreviations

SPCE	surface plasmon coupled emission
SP	surface plasmon
SPP	surface plasmon polariton
D1	Detection 1
D2	Detection 2
R6G	Rhodamine 6G
SR101	Sulforhodamine 101
TDBC	5,6-Dichloro-2-[[5,6-dichloro-1-ethyl-3-(4-sulfobutyl)-benzimidazol-2-ylidene] -propenyl]-1-ethyl-3-(4-sulfobutyl)-benzimidazolium hydroxide, inner salt
NR	Nile Red
TM	transverse magnetic
TE	transverse electric
AFM	atomic force microscopy
SERS	surface-enhanced Raman scattering

List of Publications

The main results of this thesis have been reported in the following articles:

A.I BAIEVA, S. V., HAKALA, T. K AND TOPPARI, J. J., *Strong coupling between surface plasmon polaritons and Sulforhodamine 101 dye*. Nanoscale Res. Lett.**7** (1) (2012) 191.

A.II BAIEVA, S., IHALAINEN, J. A., AND TOPPARI, J. J., *Strong coupling between surface plasmon polaritons and β -carotene in nanolayered system*. J. Chem. Phys. **138** (2013) 044707.

A.III BAIEVA, S., HOHENESTER, U., KOPONEN, M. A., HAKAMAA, O., AND TOPPARI, J. J., *About the dynamics of strongly coupled surface plasmon polaritons and Sulforhodamine 101*. Proc. SPIE Nanophotonics V **9126** (2014).

A.IV BAIEVA, S., HAKAMAA, O., GROENHOF, G., HEIKKILÄ, T., TOPPARI, J. J. , *Effect of Stokes shift on dynamics of strong coupled modes between surface plasmon polaritons and photoactive molecules*. Submitted.

Author's contribution

In A.I and II the author made all the samples and measurements. The author made the majority of data analysis and was the main writer of the publications.

In A.III the author participated in the sample fabrication and measurements. Also the first version of manuscript was written by the author.

In A.IV the author carried out the part of sample fabrication, the most of the measurements and data analysis. The author participated in the elaboration of the theoretical model and writing of the manuscript.

Contents

Chapter 1

Introduction

Since the grating anomalies discovery by R. W. Wood plasmonics has been developed into important branch of optics. Surface waves being partially oscillations of conduction electrons in metal and partially electromagnetic field are called surface plasmon polaritons (SPPs). Their fundamental properties — dispersion relation and p polarization — are derived from Maxwell's equations and boundary conditions.

The surface plasmon polariton interaction with fluorescent molecules has variety of applications such as the SPP excitation by dye emission, SPP imaging etc. But it should be taken into account that the presence of metallic interface affects the properties of emitters. In this chapter the metal film impact on decay rate and emission pattern of fluorescence molecule are considered. This changes are characteristic for weak coupling regime when emission frequency is unaffected. However in strong coupling regime the energy levels of molecule are altered in such a manner that we cannot anymore consider molecule and optical field separately. Strong coupling can be observed in many systems and some of them are discussed in this chapter.

1.1 Plasmonics

In recent decades huge attention has been devoted to the surface plasmons (SP), which are coherent oscillations of electron plasma at a metal-dielectric boundary. Their interaction with light brings many unexpected phenomena. Light coupled to the surface plasmons is responsible for strong enhancement of transmission through 2D-array of holes in metallic film (27). SPPs produced by attenuated total reflection find application as sensors (41). Strong electric field enhancement due to plasmons on rough surfaces is used in surface enhanced Raman scattering (78), fluorescence enhancement (32) and second harmonic generation (70).

The miniaturization of photonic circuits becomes realistic due to possibility to handle electromagnetic field at subwavelength scale. One of the possible scenario of such circuit performance could be following. Light is converted to SPPs by fluo-

rescent dye molecules (38) then they propagate and pass through planar optical elements such as waveguides (59), switches (62), concentrators (73), reflectors(5) and finally are converted back to light by grating. Photonic band gap system was developed for SPPs (49) and the SPP planar waveguides were used to achieve negative refraction at visible frequencies (4). Considering possible applications new branch of optics called plasmonics have arisen. It is based on microfabrication of metallic structures that can support surface waves (propagating or localized). That way it is promising to establish connection with microelectronics that relies on two dimensional lithographic techniques. Being coupled to SPPs provide possibility to develop planar optoelectronic components such as lenses (56), switches (75), directional couplers (77), *etc*. Thin metal stripes surrounded by dielectric for both guiding of SPPs and control, i.e., modulation and switching, splitting of its propagation are demonstrated (9; 63). SPP interferometer based on SPP mirror and $50/50$ beam splitter is elaborated in (26).

Nanoparticles can maintain plasmon modes called localized surface plasmons. While being illuminated with far-field light they can act as nanodimensional light sources performing excitation in the near-field region (71).

As an example of plasmonic devices involving dye molecules, one can name molecular incoupling of waveguided SPP demonstrated in (38). There SPP excitation is achieved by Coumarine 30 molecule. The excited SPPs propagate along silver waveguide about 10 μm and excite R6G molecules. In its turn R6G decays to SPPs of lower frequency. The frequency conversion efficiency yields approximately 50%. Also molecules are efficiently used as local probes of SPP's field (25). This method has advantage over scattered radiation measurement, because of wavelength conversion that leads to suppression of excitation light. In addition, tunable SPPs were employed to control ultrafast molecular electronic energy redistribution pathways in molecules on a metal surface in (85). In this study excitation of S_2 state of porphyrinic J-aggregates was done by pump pulse. When the probe pulse was tuned to excite SPP that overlaps with S_1 state of the molecules the internal conversion from S_2 to S_1 was the most efficient pathway. If the SPP energy was close to S_2 vibrational relaxation took place.

However, metal being strongly absorbing, limits SPPs propagation length and thus their applications. To overcome this problem several approaches were considered. Long range surface plasmons arise from coupling of two modes at each interface of a thin metallic waveguide (63). Another approach is introducing gain media (75). Recently the device (dye doped gold silica core-shell nanoparticles) that can generate stimulated emission of surface plasmons was proposed (64). Besides these applications SPPs serve as a good tool for material surface properties study. The strength of electromagnetic field has maximum at the surface and SPP's spectrum and lifetime strongly depend on surface quality. Thin films, defects, roughness, absorbed molecules affect it and can be studied by means of SPPs spectroscopy. One

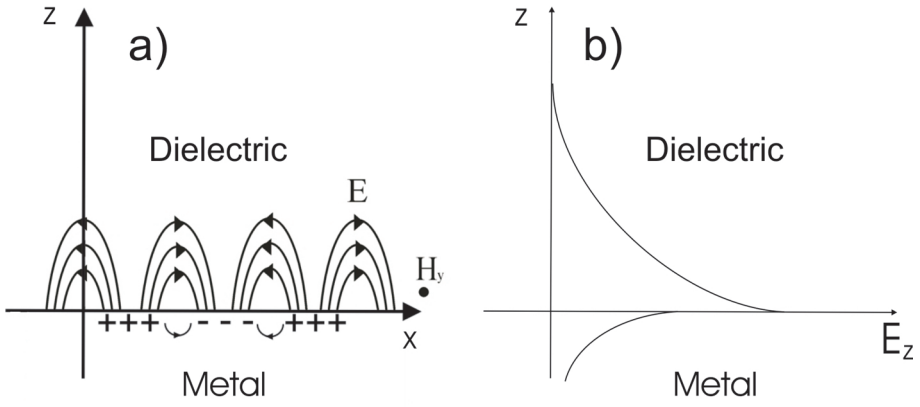

FIGURE 1.1 a) Schematic picture of the electromagnetic field and charges that are associated with SPP. b) Exponential decay of perpendicular electric field component in dielectric and metal.

version of it is based on measuring the difference in propagation length of SPPs on metal film with and without a top layer (2).

1.2 Surface plasmon polaritons (SPPs)

Surface plasmon polaritons (SPPs) are hybrid modes involving free electrons that can oscillate coherently at metal surface and light field (Fig. 1.1a). SPPs propagate in direction parallel to the interface and their electric field decays exponentially in direction perpendicular to the surface (Fig. 1.1b). During the propagation they decay due to scattering from surface imperfections and ohmic losses within the metal. Ohmic loses are due to several absorption mechanisms such as electron-electron scattering, Landau damping and absorption via intra-band transition (47).

A fundamental property of the SPPs is the dispersion relation, *i.e.*, the dependence of energy on wave vector. To describe SPPs's dispersion relation one can solve the set of Maxwell's equations for semiinfinite metal-semiinfinite dielectric system (58)

$$\bigtriangledown \times H_{m,d} = \epsilon_{m,d} \frac{1}{c} \frac{\partial}{\partial t} E_{m,d}, \tag{1.1}$$

$$\bigtriangledown \times E_{m,d} = -\frac{1}{c} \frac{\partial}{\partial t} H_{m,d}, \tag{1.2}$$

$$\bigtriangledown \cdot (\epsilon_{m,d} E_{m,d}) = 0, \tag{1.3}$$

$$\bigtriangledown \cdot (H_{m,d}) = 0, \tag{1.4}$$

where indices m and d stand for metal and dielectric layers, which are described by complex dielectric permittivitis ϵ_m and ϵ_d One can consider p (or TM in other notation) polarized light. The field is not dependent on y coordinate and according to Fig. 1.1a) for $z > 0$ it can be written as

$$\begin{aligned} H_d &= (0, H_{yd}, 0) exp[i(k_{xd}x - k_{zd}z - \omega t)], \\ E_d &= (E_{xd}, 0, E_{zd}) exp[i(k_{xd}x - k_{zd}z - \omega t)]; \end{aligned} \tag{1.5}$$

and for $z < 0$

$$\begin{aligned} H_m &= (0, H_{ym}, 0) exp[i(k_{xm}x + k_{zm}z - \omega t)], \\ E_m &= (E_{xm}, 0, E_{zm}) exp[i(k_{xm}x + k_{zm}z - \omega t)]. \end{aligned} \tag{1.6}$$

Also the boundary conditions at $z = 0$ must be fulfilled

$$E_{xd} = E_{xm}, \tag{1.7}$$

$$H_{yd} = H_{ym}, \tag{1.8}$$

$$\epsilon_d E_{zd} = \epsilon_m E_{zm}. \tag{1.9}$$

The continuity equations 1.7 and 1.8 yield

$$k_{xd} = k_{xm} = k_x. \tag{1.10}$$

From equation 1.1 it is possible to derive

$$\begin{aligned} k_{zd}H_{yd} &= -\frac{\omega}{c}\epsilon_d E_{xd}, \\ k_{zm}H_{ym} &= \frac{\omega}{c}\epsilon_m E_{xm}. \end{aligned} \tag{1.11}$$

The equations 1.11, 1.7 and 1.8 result into the system of equations

$$\begin{aligned} H_{yd} - H_{ym} &= 0, \\ \frac{k_z d}{\epsilon_d}H_{yd} + \frac{k_z m}{\epsilon_m}H_{ym} &= 0. \end{aligned} \tag{1.12}$$

The determinant of the system must be equal to zero in order to get non-zero solution and it is

$$\frac{k_{zd}}{\epsilon_d} + \frac{k_{zm}}{\epsilon_m} = 0. \tag{1.13}$$

By combining 1.1 and 1.2 relation for wave vector in metal and dielectric media can be obtained

$$k_x^2 + k_{zm,d}^2 = \epsilon_{m,d}(\frac{\omega}{c})^2. \tag{1.14}$$

Finally by solving 1.13 and 1.14 the dispersion relation for SPPs can be derived

$$k_{SPP} = k_x = \frac{\omega}{c}\sqrt{\frac{\epsilon_d\epsilon_m}{\epsilon_d + \epsilon_m}}. \tag{1.15}$$

The corresponding dispersion curve is shown on Fig. 1.2.

For s (TE) polarized light, which can be described in $z > 0$ as

$$\begin{aligned} H_d &= (H_{xd}, 0, H_{zd})exp[i(k_{xd}x - k_{zd}z - \omega t)], \\ E_d &= (0, E_{yd}, 0)exp[i(k_{xd}x - k_{zd}z - \omega t)]. \end{aligned} \tag{1.16}$$

and

$$\begin{aligned} H_m &= (H_{xm}, 0, H_{zm})exp[i(k_{xm}x + k_{zm}z - \omega t)], \\ E_m &= (0, E_{ym}, 0)exp[i(k_{xm}x + k_{zm}z - \omega t)] \end{aligned} \tag{1.17}$$

for $z < 0$. The equation 1.2 and the continuity conditions for E_y and H_x result into the relations

$$E_{ym} = E_{yd} = E_y, \tag{1.18}$$

$$E_y(k_{zm} + k_{zd}) = 0. \tag{1.19}$$

The last one can be fulfilled only if $E_y = 0$ since both k_{zm} and k_{zd} must be positive in order to have electromagnetic field described by equations 1.16 and 1.17. This means that SPPs cannot have s polarization.

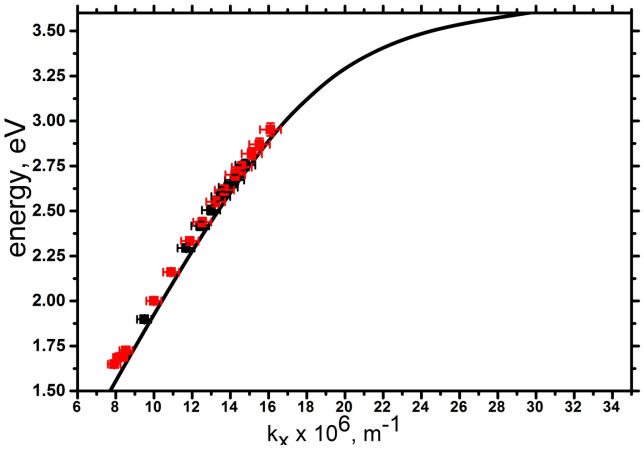

FIGURE 1.2 Dispersion of SPP at a air-metal interface (solid line). The measured dispersions obtained from reflectance (black dots) and scattered light collection (red dots) are also plotted.

In general case k_{SPP} (ω) described by 1.15 is a complex value, because the metal susceptibility is a complex number containing an imaginary part related to the absorption of radiation by the metal (ohmic loss). $Im[k_{SPP}]$ describes the internal absorption. Also $Re[k_{SPP}] > \frac{\omega}{c}$, so the components of the wave vector perpendicular to the interface between metal and dielectric k_{zm} and k_{zd} are imaginary, meaning that field amplitude decreases exponentially normal to surface. Assuming that ϵ_d is real and $Im[\epsilon_m] < |Re[\epsilon_m]|$ the skin-depth becomes (70)

$$L_m = \frac{1}{k_{zm}} = \frac{\lambda}{2\pi}\sqrt{\frac{Re[\epsilon_m] + \epsilon_d}{Re[\epsilon_m]^2}}; L_d = \frac{1}{k_{zd}} = \frac{\lambda}{2\pi}\sqrt{\frac{Re[\epsilon_m] + \epsilon_d}{\epsilon_d^2}} \tag{1.20}$$

During SPP propagation along metal-dielectric boundary its intensity decreases as $e^{-2Im[k_{SPP}]x}$ due to heat losses. In Table 1.1 important lengths are calculated for

silver-air boundary using dielectric functions measured by Johnson and Christy (46). The propagation length defines the size limit in possible planar optoelectronic circuitry. The decay length gives height limits.

TABLE 1.1 SPP's characteristic lengths in Ag-air boundary

wavelength	propagation length	decay length into dielectric	decay length into metal
500 nm	50 µm	370 nm	23 nm
1200 nm	736 µm	1650 nm	22 nm

When metal surface is rough SPPs can be coupled with photons via surface corrugations, so one can detect radiation. Another important process on the rough surface is elastic scattering between SPP modes that propagate in different directions without changing the absolute value of wave vector (19).

In order to excite SPPs with light the energy and momentum matching conditions must be fulfilled. The wave vector of incident light $\sqrt(\epsilon_d)\frac{\omega}{c}sin(\theta)$ must be equal to SPP's wave vector described by (1.15). One can calculate wave vectors for air ($\epsilon_d = 1$) and silver layers and see that SPP wave vector is larger. Therefore, special arrangements should be introduced to fulfill the excitation conditions. In Kretschmann configuration metallic layer is illuminated through a dielectric prism (for example, made of BK7 glass with dielectric constant around 2.3 for visible range) at angles of incidence greater than the critical angle of total internal reflection (70). If wave vector matching occurs light tunnels through the metal film and excites SPPs at the external metal surface. By introducing an additional dielectric layer between the prism and the metal one can excite SPPs also on internal surface of the metallic layer.

To increase the wave vector component diffraction effects can be also utilized. Diffraction grating created on a smooth metal surface can provide the momentum conservation (86). Randomly rough surface can act as diffraction grating (70). Using microscope objective with high numerical aperture one can get wide angular spread (the angles greater than critical angle of total internal reflection) of wave vectors (58).

The excitation can be done with help of fluorescent molecules that decay non-radiatively into SPPs modes via near-field. Employing dielectric prism one can make those modes radiative. The technique is called reverse Kretchmann method (35). In addition scanning near-field microscope allows excitation and probing of SPPs locally and at any place of metal structure (86). The second order imaging techniques as photochemical mapping can reveal SPP's "footprints" in photoresist (28).

1.3 Dye molecule radiation near metal interface

Spontaneous decay of molecule from excited state to the lower energy state can be accompanied with emission of a photon. Fluorescence is an example of such process.

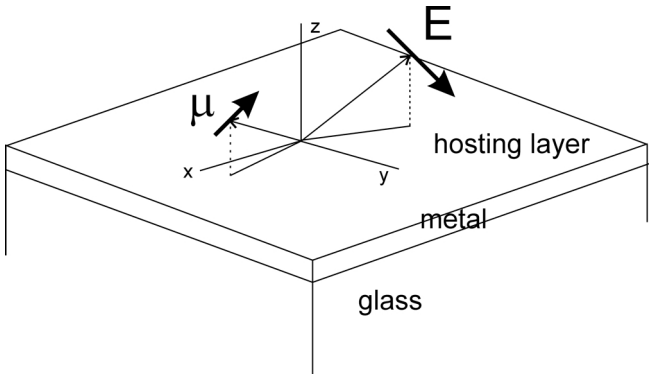

FIGURE 1.3 Dipole located in vicinity of metal layer

Usually photon absorption excites molecule to a higher electronic energy state, from which the vibrational relaxation occurs bringing molecule to "the bottom" of the excited state from where the radiative transition to other electronic state takes place. The energy of the emitted photon is equal to the energy difference of the two states. Fluorescence is described by Fermi's golden rule which tells emission probability per unit time. It dictates that transition rate is proportional to the photonic mode density.

Dye molecule can be modeled as a dipole that has certain orientation and is located at certain distance from metal film. Fig. 1.3 illustrates the case of single dipole interacting with electric field in the presence of an interface. Interface can modify radiation decay rate, quantum yield and spatial distribution of radiation (6). Additional non-radiative decay paths increase as distance to interface decrease. If the distance from the dipole is less than a wavelength dipole evanescent field components can couple to surface plasmons or lossy waves (6; 16). In (16) classical theory of dipole emission near metal interface is presented in great detail. Following reasoning in (6) one can examine decay rate of a dipole as a function of distance to the interface (Fig. 1.4). The theory predicts oscillatory behavior of decay rate that is damped as the distance to the interface increases. The interference between the initial wave and the reflected wave gives rise to the oscillations. Also fluorescence is quenched at very small distances due to the non-radiative decay to metal surface.

In order to examine changes in the radiation pattern a dipole oriented along x-axis at 40 nm above a metal film that has a thickness of 50 nm is considered. Dielectric constants are 3.25, $-14.1 + 0.4i$, 2.31 for layer hosting the molecule, metal (silver dielectric function at 570 nm) and glass substrate respectively. Far-field radiation intensity is calculated using approach presented in (66) and is plotted on Fig. 1.5. In host material layer the radiative pattern is simply horizontal dipole profile. While in glass region we observe strongly directed lobe which is called surface plasmon coupled emission (SPCE). It appears due to SPP evanescent field transformation into radiation due to the presence of glass substrate, and the high directionality comes from the conservation of SPP's momentum.

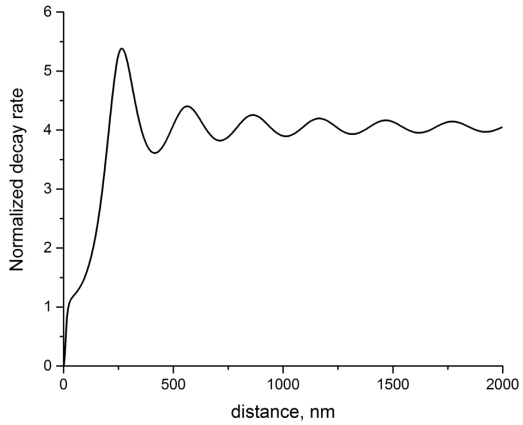

FIGURE 1.4 Normalized life time of an dipole with isotropic orientation (dipole momentum sweeps all possible orientation in space in time faster than the fluorescence lifetime (6)) in front of a silver mirror as a function of distance to the mirror. Dipole is placed in vacuum, dielectric constant of silver at 610 nm wavelength is $-16.7 + 0.47i$. Quantum efficiency of the emitting state is 0.75

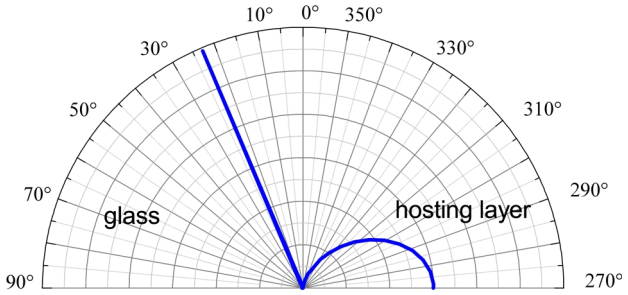

FIGURE 1.5 Radiative profile of a horizontal dipole situated in vicinity of a metal film

1.4 Strong coupling in different systems

Physics of quantum microcavities has been a hot topic in solid state physics for several decades. In quantum optical devices, microcavities can affect spontaneous emission of molecule that is hosted inside or give rise to quantum effects when spontaneous emission is fully suppressed. The optical microcavity is formed between two mirrors that are usually formed by alternate layers of high and low refractive index materials called distributed Bragg reflector (DBR). The pioneering work in observing strong coupling in monolithic solid-state system consisting of semiconductor cavity and multiple semiconductor quantum wells belongs to C. Weisbuch group (84). The most of the work in this area is based on axial confinement by DBRs, including the study of dispersion of cavity polaritons under different conditions (temperature (42), electric and magnetic fields (30; 76)).

Interaction between quantum emitter (two level system in the simplest case) and electromagnetic field in microcavity is one of the central topics of quantum electrodynamics. The lowest excited states of the uncoupled systems correspond to one photon in the cavity field mode with the emitter in the ground state, and the cavity field in the vacuum state with the emitter in the excited state. Two coupling regimes are possible. Thus in weak coupling case the spontaneous emission lifetime of quantum emitter, *i.e.* atom, changes due to Purcell effect (17), which is due to the electromagnetic mode density rearrangement within the cavity. However, damping is stronger than the light-matter interaction. In this regime the interaction between the emitter and the field is irreversible, and the energy cannot be transferred back from the emitter to cavity. However, another regime of system behavior, called strong coupling, can also be considered. The coherent coupling of an atom and the field is proportional to coupling strength

$$g_0 = (\frac{\mu^2 \omega_c}{2\hbar\epsilon_0 V_m})^{\frac{1}{2}}, \tag{1.21}$$

where μ is the transition dipole moment, ω_c is the cavity resonance frequency, and V_m is the cavity mode volume. Strong coupling requires that g_0 is larger than any decay rate and inverse of the interaction time (48). Now no irreversible energy decay takes place. Instead, the energy virtually oscillates between the emitter and photon modes (Rabi oscillations). Weak optical probing near the microcavity resonant frequency reveals two spectral transmission peaks yielding the energies of the formed new eigenstates. Strong coupling was demonstrated also for Fabry- Pérot, silica microsphere, photonic crystal microcavities (82).

The strong coupling manifests itself by separation of the degenerate eigenstates, as described above, or an anticrossing of dispersion branches and has name Rabi splitting. Splitting is significantly greater than both the excitation (exciton in quantum dots or J-aggregates) and the cavity linewidths. For a semiconductor cavity with embedded quantum wells the value of Rabi splitting is determined by oscillator strength and can be expressed as (76)

$$\Delta E = 2\hbar\sqrt{\frac{2\Gamma_0 c N_{QW}}{n_c L_{eff}}} = \sqrt{\frac{2e^2 N_{QW} f}{n_c L_{eff} \epsilon_0 m_e}}, \tag{1.22}$$

where c is the speed of light, m_e is electron mass n_c is the refractive index of cavity material, L_{eff} is an effective cavity length, N_{QW} is the number of quantum wells. Γ_0 is the radiative width of the exciton, which is proportional to oscillator strength per unite area f. Typical value of energy splitting is $5 - 10$ meV. One can see from equation 1.22 that value of splitting can be changed by tuning the cavity or exciton

properties. Besides this application of external electric and magnetic fields can affect the splitting (76). Also the splitting of in-plane polariton dispersion obtained by varying light incidence angle was studied in (43).

Lidzey *et al.* used organic semiconductor with sharp absorption band to achieve strong coupling with organic molecules for the first time (52). They tuned energy of the cavity photon by changing the angle of incidence and observed Rabi splitting up to 160 meV. The increase in splitting is attributed to large oscillator strengths of these materials ($2 \times 10^{15}\ cm^{-2}$ against $4 \times 10^{12}\ cm^{-2}$ for inorganic cavity). But the large exciton linewidth that is due to vibrational manifold complicates observation of the strong coupling. Later a considerable Rabi splitting has been achieved for dye forming J-aggregates (54).

Field enhancement of SPPs near metal surface allows observation of strong coupling without microcavity. In Kretschmann configuration strong coupling involving SPPs was demonstrated for a number of molecules including variety of J-aggregates (7; 68) and rhodamine family dyes (37; 83). The narrow absorption line and the large oscillator strength of the studied J-aggregates is very suitable for a strong coupling observation. In (7) energy splitting reached 180 meV for J-aggregates of 5,6-Dichloro-2-[[5,6-dichloro-1-ethyl-3-(4-sulfobutyl)-benzimidazol-2-ylidene]-propenyl]-1-ethyl-3-(4-sulfobutyl)-benzimidazolium hydroxide, inner salt (TDBC). Double vacuum Rabi splitting between SPP and R6G with energies 200 and 100 meV was observed in (37). In this study the dispersion relation from the scattering of the strongly coupled hybrid modes into photons was measured for the first time. It was shown that the energy splittings changed to 230 and 110 meV due to increase of the interaction time of SPPs with the molecular film (37). The change of the molecule concentration resulted in tuning of the energy gap. Square root dependence on total absorption of molecular layer was shown proving that molecules oscillate coherently in strong coupling limit. Besides Kretschmann geometry authors employed also a new approach where SPPs propagated through a molecular area on top of silver waveguide. By controlling the waveguide length the interaction time of SPP and molecules could be adjusted. For $5\ \mu$m waveguide two Rabi splits were clearly observed. The signature of spatial coherence in metal-dye molecule samples was shown in two slit experiment (36). The emission collected from spatially separated points posses interference pattern in strong coupling regime.

Also dye molecules undergo strong coupling with the SPPs modes supported by the subwavelength hole arrays (24). It was shown theoretically that strong coupling can exist between SPP and guided mode in a planar dielectric waveguide with thin metal cladding (15). This study shows that SPP propagation length can be enhanced in such structures.

Chapter 2

Theoretical description of strong coupling between SPP and dye molecules

The paradigm of strong coupling includes many approaches towards understanding of its fundamental property - the energy level splitting. Since the main topic of this study is interaction between SPPs and molecules in strong coupling limit observed with help of refractometry, the first approach considered in this chapter is based on fundamental Fresnel equations. These equations describe the light interaction with sample which in our case consists of metal and organic dye layers. One can observe transition from weak to strong coupling regime when the density of the dye molecules (that results into change of dielectric function) increases. This manifests itself as a transition from overlapping dips in the reflectance to sufficiently separated ones.

Another approach that allows describing energy splitting is based on interaction of two oscillators with energy exchange mechanism between them. The most simple system is two mechanical oscillators linked together. As a next step the eigenvalue problem that arises from quantum mechanical treatment of SPP and molecule interaction is covered. Both considered approaches result into eigenmodes that are separated in energy as long as damping is not very strong.

One more approach that leads to observation of anticrossing behavior is based on examination of SPP dispersion relation when layer of absorbing molecules is treated as damped oscillators in the electromagnetic field.

However in order to understand the strong coupling regime better full quantum mechanical models have to be invoked. In this chapter Jaynes-Cummings model is considered.It leads to the energy split dependency on electromagnetic intensity. Tavis-Cummings theoretical treatment predicts the energy gap dependence on the number of molecules.

The strongly coupled SPP- molecule excitation hybrids can scatter on the metal

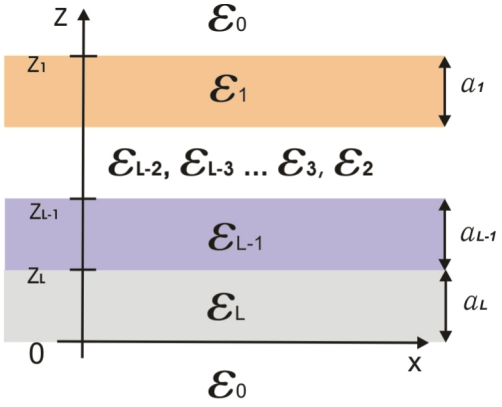

FIGURE 2.1 Schematic picture of an L-layers structure.

imperfections or decay to the molecular fluorescence. In this study the scattered radiation is employed to gain some insight into SPP-molecule interaction dynamics. As final section of this chapter theoretical approach towards modeling of SPP scattering is considered and compared to experimental findings.

2.1 Reflectance of multilayer structures

The most common method in analyzing a multilayer structure is the transfer matrix method (39). Assume that the multilayer system (Fig. 2.1) is placed within a media with dielectric permittivity ϵ_0. The layers are homogeneous and isotropic, and are described by complex dielectric function $\epsilon_l = \epsilon_l(\omega)$.

Consider p-polarized plane wave incident on the stack. The field can be described $H_{incident} = (0, H_y, 0)$. The field in l^{th} layer can be described as a superposition of reflected and transmitted waves.

$$H_l(x,z,t) = H_l^+(z)exp[i(k_{xl}x + k_{zl}z + \omega t)] + H_l^-(z)exp[i(k_{xl}x - k_{zl}z + \omega t)], \quad (2.1)$$

As a result of transformation (reflection or transmission) across the interface between $l-1$ and l layers the phase and amplitude changes occur. It can be described using phase change matrix and Fresnel equations as

$$\begin{aligned}\begin{pmatrix} H_l^+ \\ H_l^- \end{pmatrix} &= \frac{1}{2}\begin{pmatrix} exp[-ik_{zl}a] & 0 \\ 0 & exp[ik_{zl}a] \end{pmatrix}\begin{pmatrix} 1+\frac{k_{zl-1}\epsilon_l}{k_{zl}\epsilon_{l-1}} & 1-\frac{k_{zl-1}\epsilon_l}{k_{zl}\epsilon_{l-1}} \\ 1-\frac{k_{zl-1}\epsilon_l}{k_{zl}\epsilon_{l-1}} & 1+\frac{k_{zl-1}\epsilon_l}{k_{zl}\epsilon_{l-1}} \end{pmatrix}\begin{pmatrix} H_{l-1}^+ \\ H_{l-1}^- \end{pmatrix} = \\ &= T_l \begin{pmatrix} H_{l-1}^+ \\ H_{l-1}^- \end{pmatrix}. \end{aligned} \quad (2.2)$$

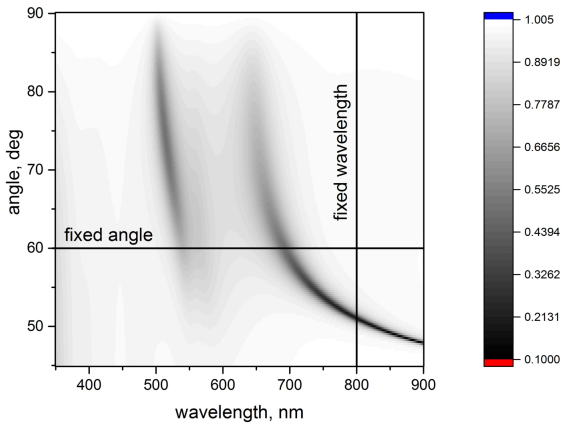

FIGURE 2.2 Reflectance coefficient of multilayer structure (air/glass/50 nm silver/ 50 nm dye molecules layer) as a function of incident angle and wavelength.

To describe the total field transformation through the stack of L layers one has to take a product of L matrices of type T_l and take into account the transformation through the surface $z_{L+1} = 0$. Reflectance coefficient can be written as

$$R = \frac{T_{21}T_{21}^*}{T_{11}T_{11}^*}, \tag{2.3}$$

where T_{ij} $(i, j = 1, 2)$ is element of total transformation matrix T that is a product of L T_l matrices.

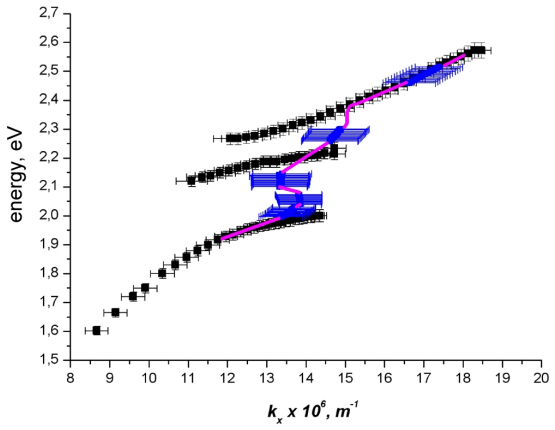

FIGURE 2.3 Experimentally obtained dispersion relation at fixed angle scans (black dots), at fixed wavelength scans (blue dots). Magenta line is a guideline for eye.

Measuring the reflectance provides a way to obtain the dispersion relation

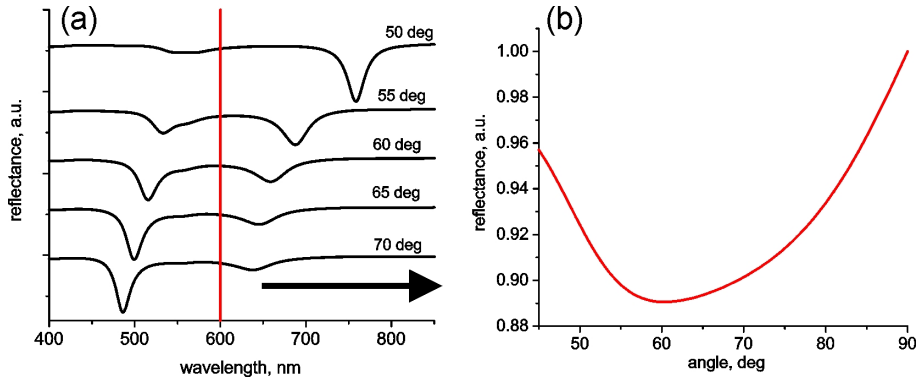

FIGURE 2.4 Calculated reflectance coefficients for air/glass/50 nm silver/50 nm dye molecules layer as a function of (a) wavelength for fixed incidence angle; (b) incidence angle for fixed wavelength. The spectra are offset for clarity in (a).

$E = E(k_x)$. Fig. 2.2 shows calculated reflectance as a function of wavelength and angle of incidence. Picking up the minima in reflectance will give the wavelength λ or energy and knowing corresponding excitation angle α one can calculate wavenumber $k = \frac{2\pi n \sin(\alpha)}{\lambda}$. There are two ways to find the reflectance minima. The first one is to perform a wavelength scan while keeping the angle of incidence fixed. The second way is to keep the excitation wavelength fixed and sweep angles. However, if one picks the angles of minimal reflectance one can get dispersion relation that has a back-bending (70) (Fig. 2.3). The finite linewidth of the hybrid modes close to the splitting region is the origin of back-bending (80). Fig. 2.4 illustrates the problem. In this work reflectance was measured by the first method and then plotted as color-scale making the problem of back-bent to disappear. In case of the strong coupling with the dye molecules, the number of molecular absorption maxima does not correspond to the number of reflectance minima (number of dispersion branches). Number of branches is always $(n + 1)$, where n is number of absorption peaks. This happens because reflectance is non-linear function of dye layer dielectric function, which is in relation with absorbance.

2.2 Strong coupling of two harmonic oscillators

Now we describe a simple model that helps to understand the frequency splitting which is indication of strong coupling. Consider two coupled harmonic oscillators in a case where there is a way to exchange energy between them. In our case surface plasmon polariton of a certain frequency is one of the oscillators and molecule with its optical transition is the other one. The simplest way to understand the concept of strong coupling is consideration of two mechanical oscillators linked together (Fig. 2.5) (65)

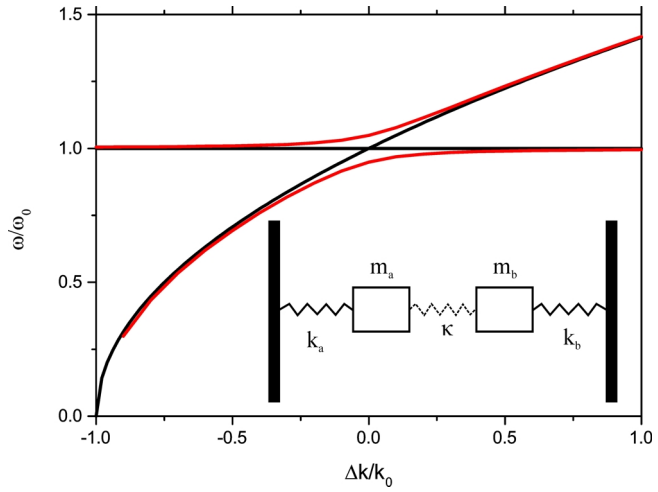

FIGURE 2.5 Eigenfrequencies of uncoupled mechanical oscillators (black curves) and coupled oscillators (red curves) .

$$\begin{aligned} m_a\ddot{x_a} + k_a x_a + \kappa(x_a - x_b) = 0, \\ m_b\ddot{x_b} + k_b x_b - \kappa(x_a - x_b) = 0, \end{aligned} \tag{2.4}$$

where $m_{a,b}$ is a mass of oscillator, $k_{a,b}$ is spring constant, κ is coupling constant.

After inserting an ansatz $x_i(t) = x_i^0 exp[-i\omega_{\pm}t]$ one can calculate eigenvalues

$$\omega_{\pm}^2 = \frac{1}{2}[\omega_a^2 + \omega_b^2 \pm \sqrt{(\omega_a^2 - \omega_b^2)^2 + 4\Gamma^2\omega_a\omega_b}], \tag{2.5}$$

where $\omega_a = \sqrt{\frac{(k_a+\kappa)}{m_a}}$, $\omega_b = \sqrt{\frac{(k_b+\kappa)}{m_b}}$, and

$$\Gamma = \frac{\sqrt{\frac{\kappa}{m_a}}\sqrt{\frac{\kappa}{m_b}}}{\sqrt{\omega_a\omega_b}}. \tag{2.6}$$

Let us set $k_a = k_0$, $k_b = k_0 + \Delta k$, $m_a = m_b = m_0$. Consider case when there is no coupling between oscillators. Eigenfrequencies become

$$\begin{aligned} \omega_+^2 = \omega_a = \frac{k_0}{m_0}, \\ \omega_-^2 = \omega_b = \frac{k_0 + \Delta k}{m_0}. \end{aligned} \tag{2.7}$$

As it can be seen from (Fig. 2.5) frequency curves intersect at $\Delta k = 0$. If there is a coupling intersection eigenfrequencies become

$$\omega_{\pm}^2 = \frac{1}{2}(\frac{k_0+\kappa}{m_0} + \frac{k_0+\Delta k+\kappa}{m_0} \pm \sqrt{\frac{\Delta k}{m_0}^2 + 4\frac{\kappa}{m_0}^2})). \quad (2.8)$$

We can set coupling $\kappa = 0.1k_0$, crossing of eigenfrequencies does not occur anymore and splitting is formed (Fig. 2.5).

If we introduce damping into equation 2.4 in a form of $\gamma_a\dot{x}$ and $\gamma_b\dot{x}$ we will get complex eigenfrequencies. The imaginary part of eigenfrequency represents linewidths. In case of strong damping the gap between real parts of eigenfrequencies decreases and eigenmodes can overlap.

2.3 Coupled oscillator model for surface plasmon polariton and molecules

Consider the multilayer structure that consists of a metal and a dielectric absorbing layers. Assume that molecules that form the dielectric layer have one optical transition, so an excitation with energy E_{Ex} and linewidth γ_{Ex} can be associated with the molecules. The set of equations describing the SPP interaction with the excitation can be written as

$$\begin{pmatrix} E_{SPP}(k_x) - i\gamma_{SPP} & V \\ V & E_{Ex} - i\gamma_{Ex} \end{pmatrix} \begin{pmatrix} \alpha \\ \beta \end{pmatrix} = \epsilon \begin{pmatrix} \alpha \\ \beta \end{pmatrix}, \quad (2.9)$$

where $E_{SPP}(k_x)$ is an energy of the uncoupled SPP at the interface between the metal layer and the dielectric matrix (without absorbing molecules), γ_{SPP} is a linewidth of SPP. Parameter V is a coupling strength between the SPP and the molecular excitation, and ϵ is an energy of the coupled state. The strong coupled modes can be described as superposition of the SPP state with probability coefficient α and molecule transition with coefficient β ($\alpha^2 + \beta^2 = 1$). If the system of linear equations has a non-trivial solution, the determinant of the system must be equal to zero. The system described by the equation (2.9) has two solutions, that describe two branches of the molecule-SPP dispersion curve

$$E = \frac{E_{SPP} + E_{Ex} - i(\gamma_{SPP} + \gamma_{Ex})}{2} \pm \sqrt{V^2 + \frac{1}{4}(E_{SPP} - E_{Ex} - i(\gamma_{SPP} - \gamma_{Ex}))^2} \quad (2.10)$$

At the resonant conditions, *i.e.*, when $E_{SPP}(k_x) = E_{Ex}$, and in the region of weak coupling $2V < |\gamma_{SPP} - \gamma_{Ex}|$ the square root is imaginary, so it describes enhancement of excitation decay rate. In the strong coupling regime, $2V > |\gamma_{SPP} - \gamma_{Ex}|$,

the square root becomes purely real and we have the difference between the upper and lower branch energies

$$\Delta E = \sqrt{4V^2 - (\gamma_{SPP} - \gamma_{Ex})^2} \tag{2.11}$$

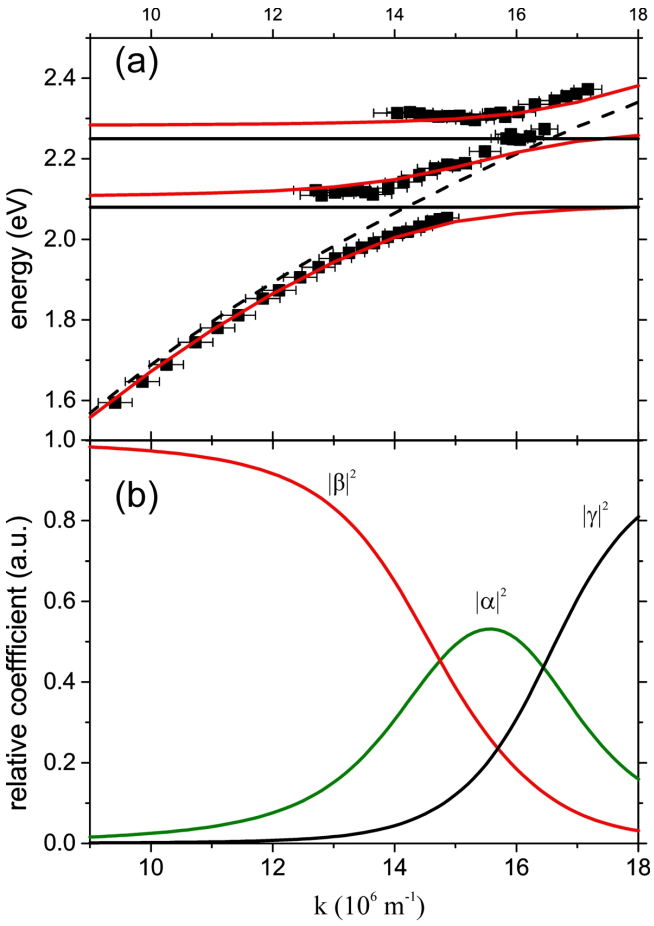

FIGURE 2.6 (a) The theoretical (red curves) and measured (black dots) dispersions (D1) for 50 nm silver - 50 nm Sulforhodamine 101 film together with Ag-SU-8 dispersion relation (dashed curve) and absorption maxima (horizontal black lines). (b) Relative weights of the middle polariton branch. Adapted from paper **III** of this thesis.

It is worth to note that for quantum microcavities one can derive similar energy splittings separately for reflected, transmitted and absorbed energy (72) . In particular, for absorption splitting in high reflectivity limit it gives

$$\Delta E_A = 2\sqrt{V^2 - \frac{1}{2}(\gamma^2 + \gamma_c^2)}, \tag{2.12}$$

where $V = \sqrt{\frac{2c\Gamma_0}{n_c L_{eff}}}$, Γ_0 is nonradiative exciton broadening, n_c is cavity refractive index, L_{eff} is sum of cavity length and length of distributed Bragg reflector, c is speed of light. Here cavity halfwidth is $\gamma_c = c\frac{1-R}{n_c L_{eff}}$, R is reflectance coefficient, γ is the nonradiative exciton broadening. When γ, $\gamma_c << V$ the Rabi splitting and absorption splitting are close to each other. According to 2.11 splitting is maximal, when the widths of excitation and SPP are equal. However, it is not the case if one considers equation 2.12.

In a case of SPP's interaction with molecule that has two absorption maxima the set of equations becomes

$$\begin{pmatrix} E_{SPP}(k_x) - i\gamma_{SPP} & V_1 & V_2 \\ V_1 & E_{Ex1} - i\gamma_{Ex1} & 0 \\ V_2 & 0 & E_{Ex2} - i\gamma_{Ex2} \end{pmatrix} \begin{pmatrix} \alpha \\ \beta \\ \gamma \end{pmatrix} = \epsilon \begin{pmatrix} \alpha \\ \beta \\ \gamma \end{pmatrix}, \tag{2.13}$$

Usually in performing fitting by coupled oscillator model we neglect the damping terms. We use SPP dispersion relation for silver-matrix interface without molecule structure obtained from measurements or calculated using transfer matrix method. Molecule transition energies are assumed to be independent of k and are deduced from reference molecular film absorption without silver. To fit data we vary coupling strength parameters V_1 and V_2. After this dispersion curves can be plotted (Fig. 2.6) as well as relative coefficients α^2, β^2 and γ^2 for each branch. To calculate the splitting values we subtract corresponding energies at k vector positions in which dispersion relation of silver-matrix SPP crosses the molecular transition energy.

It can be seen from Fig. 2.6 (b) that there is a mixing between SPP and excitations, and at the center wavevectors the middle branch contains approximately equal amplitudes of molecule transitions and surface plasmon state.

2.4 Classical and quantum mechanical description of strong coupling

Classical approach

Assume that we have emitters, *e.g.*, dye molecules, in a dielectric layer deposited on the top of a metallic layer. In order to describe dielectric function of such absorbing layer one can consider model of damped oscillator in the electric field as it is done in (80). This leads to dielectric function

$$\epsilon(\omega) = 1 + \frac{Ne^2}{V\epsilon_0 m}\frac{1}{\omega_0^2 - \omega^2 - i\gamma\omega}, \tag{2.14}$$

where N is number of molecules, e is electron charge, V is volume, m is electron mass and γ is damping factor. Consider equation (1.15) taking into account several assumptions. Assume that metal dielectric function ϵ_m is constant. In optical range it is negative and large (46) in comparison to ϵ_d, so denominator of the dispersion relation has negligible frequency dependence. After momentum scaling to $\kappa^2 = k^2 \frac{|\epsilon_m + \epsilon_d| c^2}{|\epsilon_m|}$ one obtains

$$(\kappa - i\frac{\gamma_{SPP}}{2})^2 = \omega^2(1 + \frac{\frac{Ne^2}{V\epsilon_0 m}}{\omega_0^2 - \omega^2 - i\gamma\omega}), \tag{2.15}$$

where γ_{SPP} describes SPP final linewidth. In the case when we are close to resonance ($\kappa, \omega \approx \omega_0$) we get $\kappa + \omega \approx 2\omega_0$, $\omega_0 + \omega \approx 2\omega_0$. And after rearrangement the equation (2.15) results into

$$(\kappa - i\frac{\gamma_{SPP}}{2} - \omega)(\omega_0 - \omega - i\frac{\gamma}{2}) = \frac{Ne^2}{4V\epsilon_0 m}. \tag{2.16}$$

As a solution of equation (2.16) one has two normal modes

$$\omega_\pm = \frac{\kappa}{2} + \frac{\omega_0}{2} - i\frac{\gamma_{SPP}}{4} - i\frac{\gamma}{4} \pm \frac{1}{2}\sqrt{\frac{Ne^2}{V\epsilon_0 m} + (\kappa - \omega_0 - i\frac{\gamma_{SPP}}{2} + i\frac{\gamma}{2})^2}, \tag{2.17}$$

which at the resonance ($\kappa = \omega_0$) becomes

$$\omega_\pm = \omega_0 - i\frac{\gamma_{SPP}}{4} - i\frac{\gamma}{4} \pm \frac{1}{2}\sqrt{\frac{Ne^2}{V\epsilon_0 m} - (\frac{\gamma}{2} - \frac{\gamma_{SPP}}{2})^2}. \tag{2.18}$$

The normal mode splitting thus becomes

$$\Omega = \sqrt{\frac{Ne^2}{V\epsilon_0 m} - (\frac{\gamma}{2} - \frac{\gamma_{SPP}}{2})^2}. \tag{2.19}$$

It is proportional to concentration of emitters and reduced by damping. The complex frequency described by equation 2.18 leads to the situation when the part of function describing oscillations $exp(-i\omega t)$ will include damping term $exp(-\frac{(\gamma_{SPP}+\gamma)t}{4})$. In order to observe strong coupling phenomena the strength of the coupling should be greater than the linewidth of damped mode, which is the sum of absorption resonance and plasmonic resonance widths $\frac{\gamma}{2} + \frac{\gamma_{SPP}}{2}$. This leads to the inequality

$$\frac{Ne^2}{V\epsilon_0 m} > \frac{\gamma^2}{2} + \frac{\gamma_{SPP}^2}{2}. \tag{2.20}$$

Quantum mechanical approach

Here we consider quantized electric field interacting with single quantum mechanical emitter. The system is described by so-called Jaynes-Cummings Hamiltonian (60)

$$\hat{H} = \hat{H}_0 + \hat{H}_I = \overbrace{\frac{1}{2}\hbar\omega_0\sigma_z + \hbar\omega\hat{a}^\dagger\hat{a}}^{\hat{H}_0} + \overbrace{\hbar g(\hat{a}\sigma_+ + \hat{a}^\dagger\sigma_-)}^{\hat{H}_I}, \tag{2.21}$$

where σ_z, σ_+ and σ_- are Pauli matrices, $\hat{a}$ is SPP annihilation operator, $\hat{a}^\dagger$ is creation operator and g is coupling strength. In case of time-dependent interaction Hamiltonian wave-function could be found from

$$i\hbar\frac{\partial|\phi\rangle}{\partial t} = \vartheta|\phi\rangle, \tag{2.22}$$

where $\vartheta = e^{\frac{i\hat{H}_0 t}{\hbar}}\hat{H}_I e^{\frac{-i\hat{H}_0 t}{\hbar}}$, which becomes

$$\begin{aligned} \vartheta = g\hbar(\hat{a}\sigma_+ e^{i\delta t} + \hat{a}^\dagger\sigma_- e^{-i\delta t}), \\ \delta = \omega - \omega_0. \end{aligned} \tag{2.23}$$

The possible states of emitter are ground state g or excited state e and there can be n SPPs. So the eigen states are $|g,n\rangle$ and $|e,n\rangle$. Using probability amplitude method one can write wavefunction as

$$|\phi\rangle = \sum_n [C_{g,n}(t)|g,n\rangle + C_{e,n}(t)|e,n\rangle]. \tag{2.24}$$

Equation (2.22) results into the system of equations

$$\frac{\partial C_{g,n}}{\partial t} = -ig\sqrt{n+1}e^{i\delta t}C_{e,n+1} \tag{2.25}$$

$$\frac{\partial C_{e,n+1}}{\partial t} == -ig\sqrt{n+1}e^{-i\delta t}C_{g,n}. \tag{2.26}$$

Solving (2.25),(2.26) together with boundary conditions $C_{g,n}(0) = C_0$ and $C_{e,n+1}(0) = 0$ one ends up with probability amplitudes

$$C_{g,n}(t) = C_0(cos(\frac{\Omega_n t}{2}) - i\frac{\delta}{\Omega_n})sin(\frac{\Omega_n t}{2})e^{\frac{i\delta}{2}}$$

$$\mathrm{C}_{e,n+1}(t) = -\frac{2ig}{\Omega_n}\sqrt{n+1}sin(\tfrac{\Omega_n t}{2})e^{\frac{-i\delta}{2}}, \tag{2.27}$$

where the generalized Rabi frequency becomes

$$\Omega_n = \sqrt{\delta^2 + 4g^2(n+1)}. \tag{2.28}$$

If $n = 0$ there is the splitting even if there are no electromagnetic quanta. It is called the vacuum Rabi splitting and it is due to the electromagnetic vacuum fluctuations.

In case of N emitters, with the same transition frequency ω_0, quantum mechanical model is extended and it is described by Tavis-Cummings Hamiltonian

$$\hat{H} = \hbar\omega\hat{a}^\dagger\hat{a} + \hbar\omega_0 J_z + \hbar\frac{\lambda}{\sqrt{N}}(J_+\hat{a} + J_-\hat{a}^\dagger), \tag{2.29}$$

where $J_z = \sum_{i=1}^{N}\sigma_{z,i}$, $J_+ = \sum_{i=1}^{N}\sigma_{+,i}$, $J_- = \sum_{i=1}^{N}\sigma_{-,i}$, where i denotes emitter number, and the collective coupling $\lambda = \sqrt{N}g$, where N is number of molecules. Hamiltonian (2.29) commutes with total number of excitation in system $\hat{n} = \hat{a^\dagger}\hat{a} + J_z$ and diagonalization can be done using its eigenvectors as basis (14). In case of $n = 0$ there is only one eigenstate $|g...g;0\rangle$ where all emitters are in the ground state and there is no SPP. In case of $n = 1$ the basis is formed by state $|g...g;1\rangle$ and N different states $|g...e_i...g;0\rangle$ with only one emitter excited. Diagonalization gives two polaritonic eigenstates

$$|+\rangle = \cos\phi|g...g;1\rangle + \sin\phi\frac{1}{\sqrt{N}}\sum_{i=1}^{N}|g...e_i...g;0\rangle \tag{2.30}$$

$$|-\rangle = -\sin\phi|g...g;1\rangle + \cos\phi\frac{1}{\sqrt{N}}\sum_{i=1}^{N}|g...e_i...g;0\rangle, \tag{2.31}$$

where

$$\tan(2\phi) = \frac{2\lambda}{\omega-\omega_0}. \tag{2.32}$$

The corresponding eigenenergies are

$$E_\pm = \hbar\frac{\omega+\omega_0}{2} \pm \hbar\sqrt{\lambda^2 + \frac{(\omega-\omega_0)^2}{4}}. \tag{2.33}$$

The rest of the N eigenstates are combinations of $N-2$ states $|g...e_i...g;0\rangle$ without overlap with SPP excited state. They are called dark states, because they cannot be reached from the ground state $|g...g;0\rangle$ by exciting SPP mode. The important result here is that energy splitting is proportional to $g\sqrt{N}$.

2.5 Theory about scattering

Once created, SPPs can decay radiatively due to interaction with electron density fluctuations in metal, *e.g.* dislocations, grain boundaries etc. In general surface structure is characterized by two parameters: the root-mean-square variation in the height δ and average distance over which surface structure is correlated σ. δ^2 determines the strength of radiative decay of SPPs, while σ determines the average amount of momentum transferred between SPP and the surface (12).

In most of the theories intensity profile is considered as product of two functions. One is angle dependent function which is result of Maxwell's equation solution with certain boundary conditions. And other one is surface momentum spectrum.

In Kretschmann's study surface plasmons are excited by prism coupling technique and they are modeled as dipole emitters in air (51). The radiation pattern is product of dipole emission function and roughness spectrum of the surface. Examples of dipole emission patterns calculated using formulas derived in (51) are shown on Fig. 2.7. However, in (12) three different patterns for p-polarized radiation were observed in case when the plane of incidence coincides with observation plane on Fig. 2.8. Some of them differ from the one on Fig. 2.7 by presence of lobes in both quadrants. Also s-polarized radiation was collected for both detection

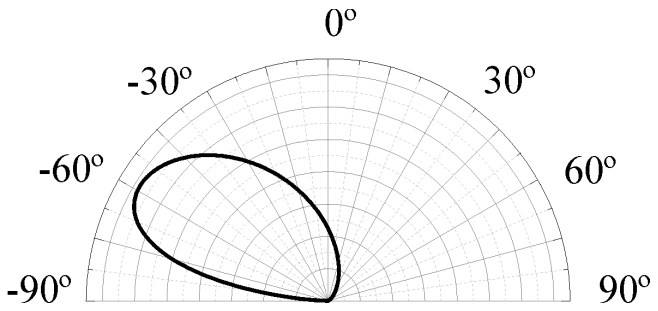

FIGURE 2.7 The radiative pattern of a dipole on the air-silver boundary. The plane of incidence coincides with the plane of observation.

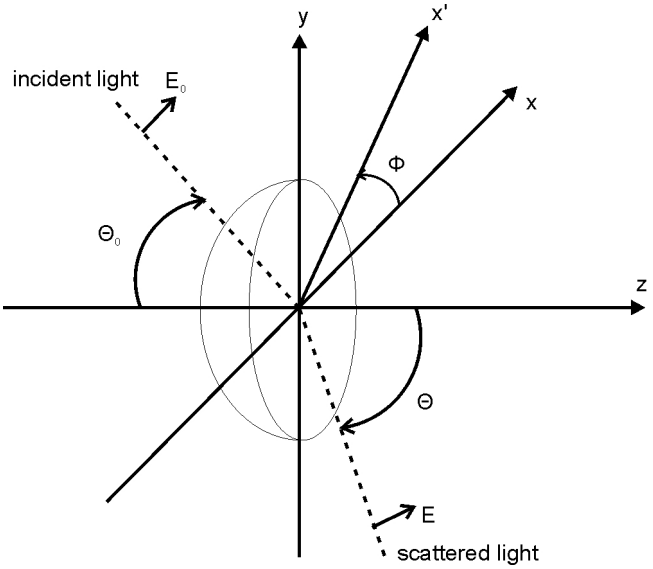

FIGURE 2.8 Schematics of experimental geometry. Light is incident in (x',z)-plane, SPP radiation is observed in (x,z)-plane. The angle between these planes is Φ. θ_0 is incidence angle and θ is observation angle.

planes parallel with respect to plane of incidence and perpendicular observation plane (10; 12), while Kretschmann's theory predicts no s-polarized intensity when plane of incidence coincides with observation plane. In (10; 12) authors claim that the δ parameter was approximately the same for all studied films, but the key to the radiation patterns difference is σ parameter . Their picture of SPPs scattering is following. SPPs are scattered in different directions by surface irregularities, but efficient back-scattering is due to grain boundaries. The surface momentum function in their consideration consist of two components, which describe low and high momentum transfers. To find good fit to their experimental results authors develop in (11) the model which is based on application of boundary conditions (tangential components of electric and magnetic field are continuous) to the sum of incident and scattered field. The later is presented as series of small parameters. However, used autocorrelation functions lead only to single lobed or diffuse patterns.

All previous studies consider the case of SPP excitation with monochromatic

light and measuring the radiative pattern as a function of angle of emission from the film surface. According to (13) radiation pattern in the far-field can be described as

$$P(\theta) = \frac{A}{\lambda^4} F(\theta) g(k_s), \tag{2.34}$$

$$F(\theta) = \frac{|\sqrt{\cos^2(\theta) - \epsilon} - \sqrt{-\epsilon}\cos(\theta)|^2}{\cos^2(\theta) - \epsilon \sin^2(\theta)} \sin^2(\theta), \tag{2.35}$$

where ϵ is silver frequency dependent dielectric function and θ is detection angle. The Fourier transform of surface autocorrelation function is

$$g(k_s) = \pi \delta^2 \sigma^2 exp(-\frac{\sigma^2 k_s^2}{4}), \tag{2.36}$$

where

$$k_s = \frac{2\pi}{\lambda} \sqrt{\epsilon sin^2(\theta_0) + sin^2(\theta) - 2\sqrt{\epsilon} sin^2(\theta_0) sin^2(\theta) cos(\phi)}, \tag{2.37}$$

here λ is SPP excitation wavelength, θ_0 is the excitation angle, ϕ is angle between plane of incidence and plane of observation.

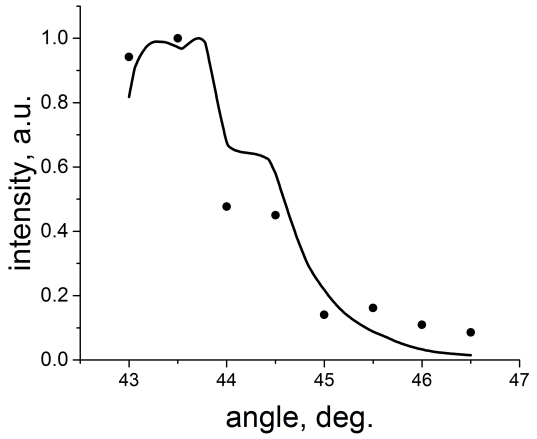

FIGURE 2.9 Measured (black dots) and calculated (solid line) dependence of scattered intensity on incident angle for silver-air structure. $\sigma = 0.2\mu m$. The data are normalized.

In our studies the SPPs were excited with white light radiation and we collected scattered radiation with collimating optics assembly placed normal to the

surface. The field of view of collection optics is estimated to be around $3°$. The observation plane coincide with the excitation plane. We used formulas (2.34)-(2.37) to estimate SPPs scattered radiation dependence on excitation angle. For this purpose we integrated 2.34 in field of view limits and compared it to measured scattered radiation intensity in Fig.2.9. As one can see theoretical scattered intensity dependence describes experimental result reasonably.

Chapter 3

Experimental study of SPP-molecule interaction in strong coupling regime

In this chapter the experiments that show a strong coupling between SPPs and organic dye molecules are presented. The measurements were done in Kretschmann configuration with white light excitation. Dispersion relations were deduced from reflected and scattered signals. The changes in the dispersion relation obtained by two methods are discussed. Also the reverse Kretschmann configuration was employed to collect surface plasmon coupled emission.

3.1 Strong coupling between Sulforhodamine 101, β-carotene and SPPs

Interaction between SPPs and emitters, such as fluorescent molecules and quantum dots, is topic of various studies nowadays (7; 18; 35). In many cases interaction is governed by Fermi's Golden rule and thus considered to be in weak coupling regime. In this regime the powerful technique of SPPs propagation imaging operates which is based on fluorescent molecules excited by SPP's evanescent field (58). Also enhancement of the molecular fluorescence via Purcell factor due to coupling to plasmon happens in weak coupling(45). However, in the strong coupling regime the interaction between SPP and molecule cannot be anymore explained in terms of absorption and emission. This gives rise to an anti-crossing behavior in dispersion relation.

We observed the anti-crossing of energy levels in case of Sulforhodamine 101 (SR101) coupling to SPPs. SR101 is an organic semiconductor which has two absorption maxima at 555 nm (2.33 eV) and 600 nm (2.07 eV) (deduced from thin film absorption spectrum). The studied samples consisted of a thin silver layer evaporated on the glass substrate, and a homogeneous organic semiconductor layer formed on the top of that. The excitation of SPPs was done by prism coupling technique and

Rabi splittings, with energy gaps up to 360 and 190 meV, were obtained. We used both the coupled oscillator model and the transfer matrix method to fit the experimental results. Also the scattered radiation of the propagating strongly coupled SPP-molecular exciation hybrids was used for studying the dynamics and mode emission after the incoupling. Because of the propagation of the hybrid polaritons before scattering, the scattering event is spatially and temporally separated from the incoupling.

Besides strong fluorescent dyes we investigated one of the natural pigments - β-carotene. It is a light-harvesting pigment in the photosynthetic system of plants absorbing and transferring energy to chlorophylls. Also, it functions as a protector against excessive light by quenching both singlet and triplet states of chlorophylls. Besides photosynthesis, it is efficient quencher of dangerous singlet oxygen and various other reactive radicals. The first excited state S_1 is a "dark" state due to the molecule symmetry. Thus the conventional absorption and fluorescence spectroscopy observe transitions involving second excited state, conventionally called S_2 (69). A lot of effort is done to locate and understand the role of the S_1 state. In our study we did not see indications of S_1 state.

Below we demonstrate strong coupling between SPPs and the S_2 state of β-carotene. Additionally, we excited the molecule by laser and measured the emission patterns revealing clear surface plasmon coupled fluorescence (SPCE). Carotenoids have strong vibrational states resulting in intense resonance Raman signals (40). Raman spectra were also measured in strong coupling limit.

3.1.1 Experimental details

Fabrication of the silver layer

The sample was made of 55 nm of silver deposited on a glass substrate by electron-beam evaporation in ultra high vacuum (10^{-8} mbar). The choice of the metallic film thickness is done by finding the minimum of reflectivity as a function of the metal thickness (Fig. 3.1). Contrary to (46), where evaporation rate was chosen to be 6 nm/s, the evaporation rate used here was $0.02-0.04$ nm/s to obtain smooth surface (2.5 nm RMS roughness). We verified the silver thickness and quality by atomic force microscope (AFM). In (55) silver film surface roughness was reduced by means of evaporation of several nm thick nickel layer. We also tested this method but did not see improvement in terms of surface roughness or grain size.

Molecules-resist layer

Altogether, six samples with different SR101 concentrations were prepared as well as a reference sample without SR101. SU-8 epoxy-based negative photopolymer resist was used as a matrix for the molecules. Desirable amount of SR101 was firstly

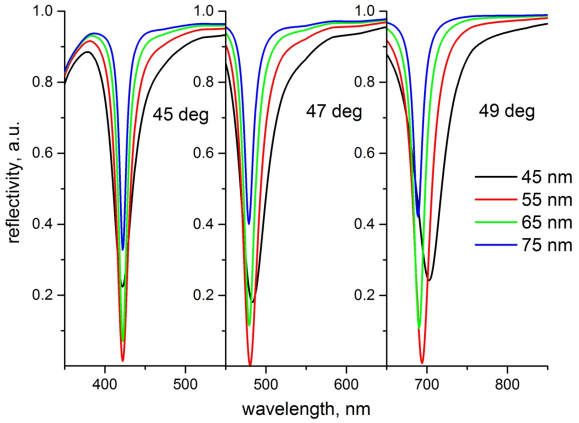

FIGURE 3.1 The reflectivity of glass/silver structure plotted as a function of excitation wavelength at several excitation angles and layer thickness. In every angle the minimum occurs for a thickness of 55 nm

dissolved in ethanol. After that the obtained solution was mixed with SU-8 solution in cyclopentanone. Further filtering was used to remove aggregates with the size above 0.2 μm. After the filtration, the resist was spin coated on top of the silver and baked at $95°C$. In order to obtain resist thickness of approximately 55 nm, the spinning rate of 4500 rpm was used for 45 s. It was also found that the resist layer protected the silver against the oxidation process. The samples containing R6G and NR were fabricated in similar way as SR101 samples.

Samples containing TDBC molecules were fabricated in following way. Desirable amount of molecule ($0.8 - 3.4$ mg) was dissolved in 500 μl of water. Then 250 μl of Polyvinyl alcohol solution in water (5% by weight) were added. The layer was spin-coated with 4500 rpm rate for 45s. No baking was done.

Reference samples for the absorption measurement without silver were similarly fabricated. The absorbance spectra measured by Perkin Elmer UV/VIS Lambda 850 spectrometer are shown in Fig. 3.2(a).

Using absorbance (or transmission) data one can calculate imaginary part of refractive index (absorption index)

$$\kappa = \frac{-ln(T)\lambda}{4\pi D}, \tag{3.1}$$

where T is a transmission of the sample, λ is a wavelength, D is a sample thickness. The absorption index is linked to the dielectric function ϵ of molecular layer via following relations

$$Re(\epsilon) = n^2 - \kappa^2, \; Im(\epsilon) = -2n\kappa, \tag{3.2}$$

where n is a real part of refractive index. We assume that the dielectric function is a combination of Lorentzian curves. In order to get the parameters that describe these curves we fit experimental absorption index with calculated one.

The SPP dispersion relation is strongly dependent on thicknesses of the silver and the dielectric layers, and silver quality, in addition to the dye molecule concentration. In order to compare the dispersion relations of samples with different dye concentrations, we kept all the other parameters unchanged.

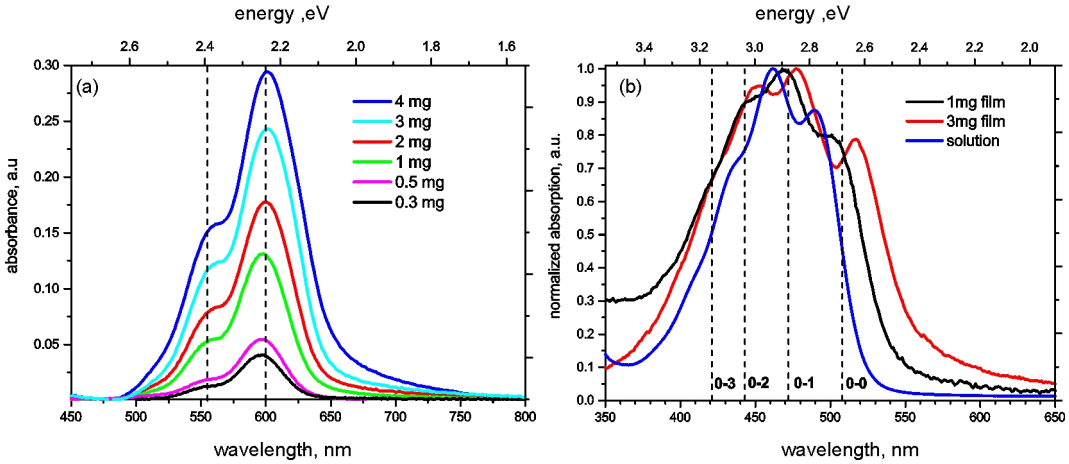

FIGURE 3.2 Absorptions of (a) SR101, (b) β-carotene samples.

For the experiments with β-carotene we prepared samples that contained 1 and 3 mg of molecule dissolved in 1 ml of chloroform. After that the obtained solution was mixed with 10 μl of SU-8 resist already diluted in cyclopentanone. The film was spin-coated at 4500 rpm for 1 minute resulting in 40 nm thickness, measured with AFM. In the case of β-carotene the baking was avoided because it led to an extended β-carotene aggregation. Reference sample absorptions are shown on Fig. 3.2(b). The overall redshift of the thin film spectra as compared to the highly diluted solution spectrum is most likely due to a J-aggregate formation. The tendency of formation of H- and J-aggregates in hydrated polar solvents is well-known for carotenoids (8; 87) and is controlled by solvent properties and molecule concentration. For the further modeling, the absorption spectrum of the β-carotene film was fitted with four Lorentzian curves associated with four vibrational bands of the $S_0 \rightarrow S_2$ transition. The peaks are located at 508 (0-0 transition), 472 (0-1), 443 (0-2), and 421 nm (0-3) for the less concentrated film.

Measurement setup

In Fig. 3.3 the schematics of the experimental setup is shown. For the excitation of SPPs a collimated white light beam is incident onto the sample surface through a hemicylindrical glass prism (Kretschmann configuration). The prism is made of

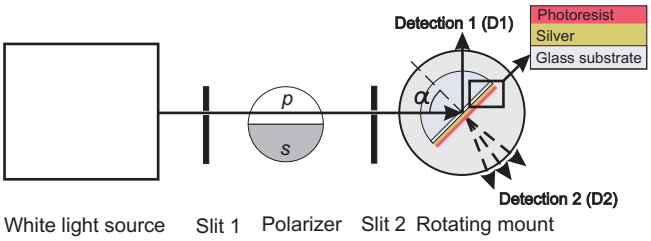

FIGURE 3.3 Schematic picture of the measurement setup and sample.

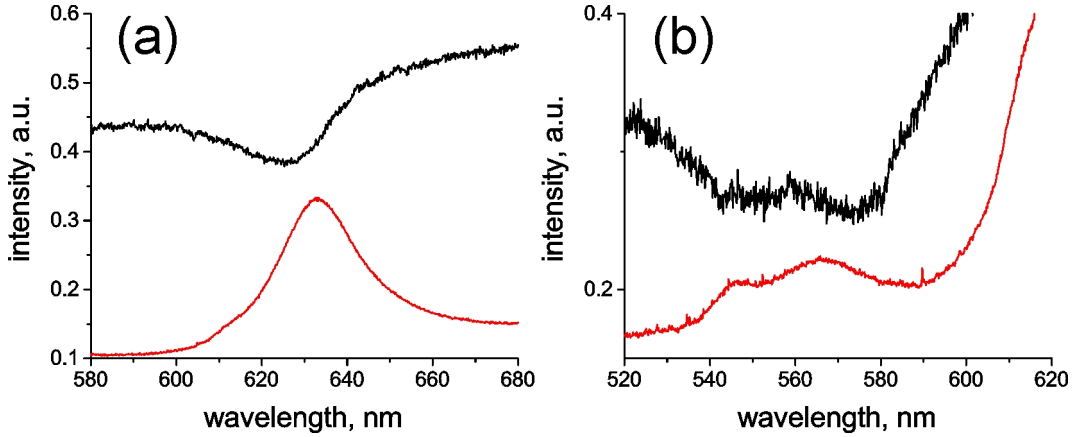

FIGURE 3.4 Measured D1 (black curves) and D2 (red curves) spectra for 1mg SR101 sample. Detection angle is 79°. In order to collect D2 signal presented in (b) exposure time was increased in 2.5 times in comparison to (a).

BK7 glass with the index of refraction of 1.52. The sample was installed on the flat face of the prism by index matching oil with the same refractive index, and Oriel 66182 white light source was used for the excitation. The light was collimated and aligned by two slits and the polarization was adjusted by a rotatable Glan-Taylor prism polarizer. The excitation light was always adjusted to p-polarisation to avoid extra background due to s-polarized light, which does not excite SPPs. The incident angle of the incoming light was adjusted manually by a goniometric prism mount. The reflected (D1) and scattered (D2) signals were collected by an optic fiber connected to Jobin Yvon iHR320 spectrometer equipped with Jobin Yvon Symphony CCD camera. It should be noted that the reflected and scattered signals were not collected simultaneously.

In Kretschmann geometry one can vary the wave vector component that is parallel to the interface

$$k_{x,light} = \frac{\omega\sqrt{\epsilon_{prism}}}{c} sin(\alpha), \tag{3.3}$$

where ω is the excitation frequency, ϵ_{prism} is the dielectric permittivity of the prism and glass substrate and α is the angle between the normal to the sample surface and

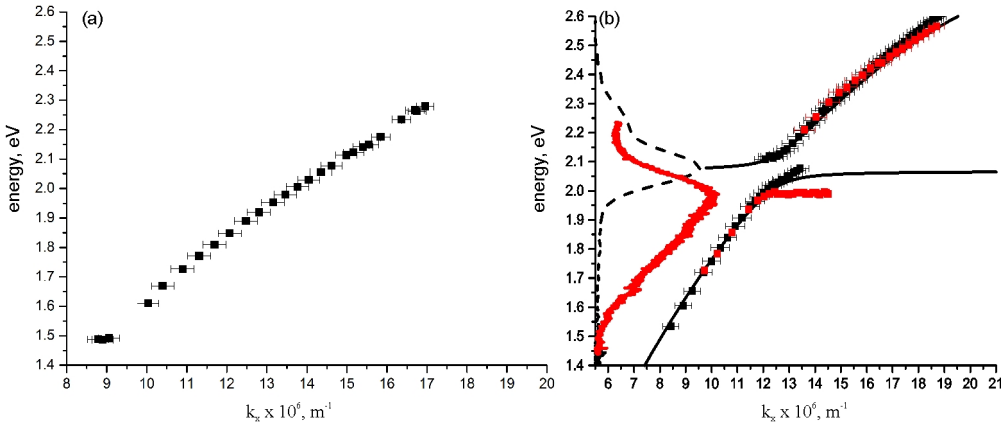

FIGURE 3.5 Measured dispersion curves for (a) silver-SU8 sample, (b) silver-SR101 of lowest concentration. Black and red dots are dispersion obtained using D1 and D2 data respectively. Solid black line is coupled oscillators model fitting. Black dash and red lines represent SR101 film absorption and emission spectra respectively.

the normal to the wave front, *e.g.*, the angle of incidence. x-axis is chosen to be along the silver surface within the plane of incidence of the excitation light. The incoupled energies are visible as dips in the reflected signal. The dispersion relation was obtained by measuring spectra and determining the energies of those dips at a range of the incident angles. In addition, we used also detection of the radiation scattered on the molecular side of the sample in order to get the dispersion relation. SPPs or SPP-molecule polaritons scatter to far field photons on silver film corrugations and the peaks of intensity in the scattering spectrum were observed in D2. An example of measured data is shown on Fig. 3.4.

3.1.2 Strong coupling and vacuum Rabi splitting

For the investigation of the dependency of dispersion relation on SR101 concentration a sample without any dye molecule was first measured in D1 geometry. As it can be seen from Fig.3.5 (a) the obtained dispersion curve is continuous. When the molecule is added (samples containing less than 1 mg SR101) an energy gap appears at the position of the lower absorption maximum (Fig. 3.5 (b)). By increasing the concentration, this gap widens and a second gap, corresponding to the absorption shoulder, opens. With an increasing concentration both energy gaps widen as it can be seen from Fig. 3.6 (a). For the lowest concentration sample we were able to measure also the SR101 fluorescence in D2 geometry besides the SPP dispersion (red dots that form horizontal part of the dispersion branch in Fig. 3.5 (b)). This could indicate that the strong coupling limit has not been fully reached yet despite the Rabi splitting observed. The hybrid polariton modes can also decay to uncoupled SPPs or excited molecules which subsequently fluoresce (50). However, this can as well

be indication that not all the molecules are strongly coupled to SPPs, which is easily understood by the random orientation of the molecules. The vertically oriented dipoles are coupled strongest while the horizontal are not coupled at all (6). Otherwise the behavior of the dispersion is similar to D1 case except energy separations of the opened gaps are larger as explained earlier (37).

We verified the independency of the gap width on the excitation light intensity by measuring dispersion curves of silver-β-carotene sample at different illumination levels. For this purpose we employed neutral density filter to adjust the light intensity. Fig. 3.7 shows the results proving the absence of any dependence on the intensity. The independence on the excitation intensity indicates that we are always on the limit of molecules interacting maximum with one SPP at the time. This means that the gaps on the dispersion relation can be called vacuum Rabi splittings and they separate new independent eigenstates of the system regardless of the occupation of the states. The white light source we used in this study provide low fluence, so the average occupation number is less than unity. Also it should be noted that significant portion of molecules remains uncoupled, because the SPP field is localized to small volume near the interface.

For D1, the lower and the upper energy gap values are linearly dependent on the square root of the total absorbance or in other words on the effective oscillator strength of the molecule ensemble (Fig. 3.6 (a) and (b) inset). The total absorbance is obtained by integrating the absorbance spectrum of the reference sample without silver. The lower energy gap value changes from 200 to 330 meV when the amount of SR101 changes from 1 to 4 mg. Meanwhile, the upper energy gap value varies from 90 to 190 meV. The data obtained from D2 shows larger values for the lower energy gap in comparison to D1. Namely, the lower gap value now changes from 220 to 360 meV. The linear dependence on the square root of the total absorbance still holds.

To understand the increase of the lower energy gap one may reason in following way. Consider equation (2.11) which describes the interaction of SPP with single excitation. For the case of two excitations the expression gets more complex, but the general features can still be traced. The term $V \propto (absorbance)^{\frac{1}{2}}$ is responsible for the gap increase. In the case of reflectance, D1, the photon-SPP has a limited interaction time with molecules until reflected back to the detector. During this time, the SPP does not reach its full spatial coverage determined by the propagation speed and the decoherence time and, thus, only interacts with a limited number of molecules making the oscillator strength effectively smaller. However, in D2, we detect scattered SPPs, which have propagated along the silver-SR101 resin boundary, and the spatial coverage of the SPP has reached its full value, thus, enabling more dye molecules to be involved in the interaction process, which further increases the effective oscillator strength. In the other words, the interaction time has also increased. This same can also be interpreted as decreased $(\gamma_{SPP} - \gamma_{Ex})$ term in (2.11). In D1 case the interaction

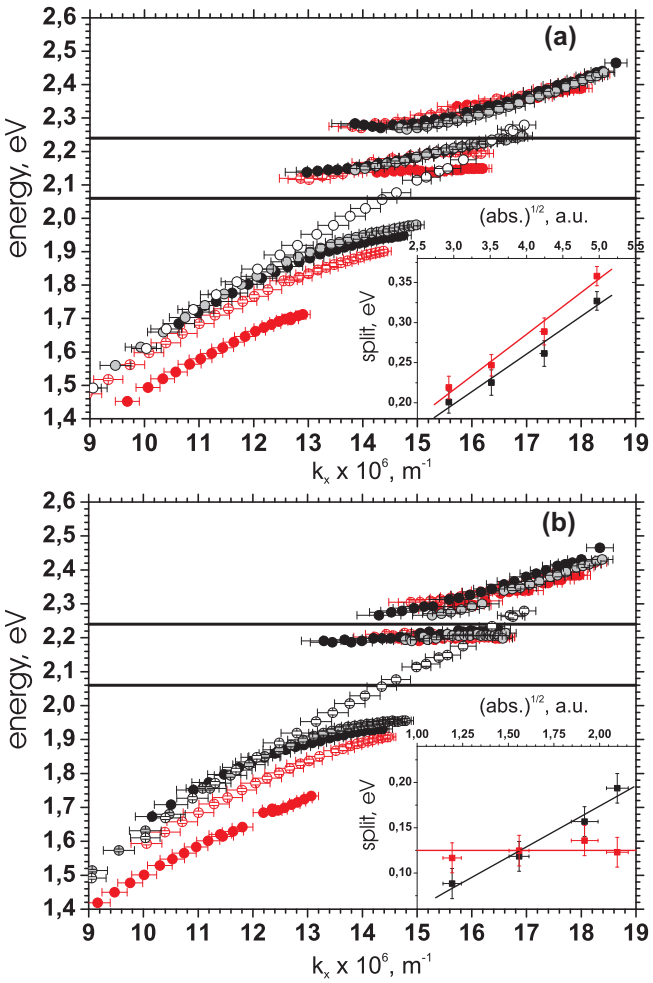

FIGURE 3.6 Measured dispersion curves and the Rabi energies. The dispersion curves of the four samples having 1 mg SR101 (solid gray circles), 2 mg (solid black circles), 3 mg (empty red circles), and 4 mg (solid red circles) measured by D1 (a) and D2 (b) geometries. The empty black circles represent the dispersion relation of the sample without SR101 molecule measured at D1. Solid black horizontal lines are the SR101 absorption maximum and the absorption shoulder energies. The insets show the low (a) and high (b) energy splits as a function of $(absorbance)^{\frac{1}{2}}$ with linear fits. Black dots correspond to D1, and red dots correspond to D2. Adapted from the paper **I** of the thesis.

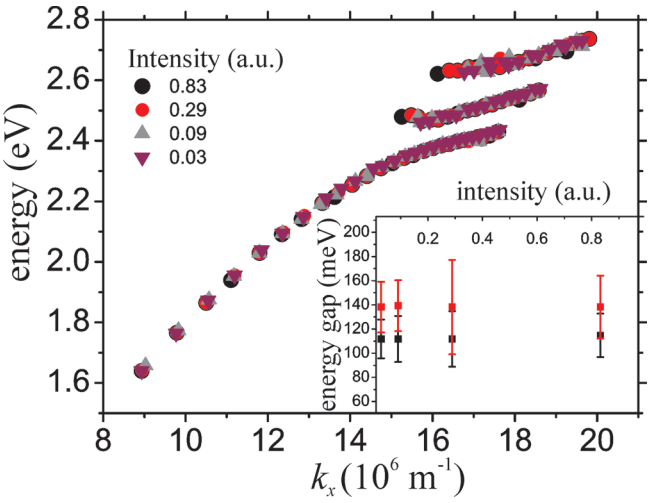

FIGURE 3.7 Dispersion relations of β-carotene sample with 1 mg of molecule, measured at different excitation light intensity levels. Inset shows energy gaps as a function of light intensity (transmission value of the neutral density filter).

time is short and it is equal to the time of metal response to photon field. In contrast, for D2, the interaction time of SPPs with the molecular film is only limited by the decay or scattering of SPP. This concept is proven in (37) by preparing samples with variable molecular layer length.

Contradicting the above reasoning the upper energy gap is independent on the samples absorbance and stays close to 125 meV in the case of D2. This tendency can find the explanation via considering the role of the SPP lifetime that is proportional to ${\gamma_{SPP}}^{-1}$. This means that shortening of the SPP lifetime decreases the Rabi split via increasing γ_{SPP} and could thus compensate the increase in V resulting from the increased SR101 concentration. The shortening of the lifetime of the upper polariton branch can be due to increased exciton-phonon scattering, which can cause population transfer from the upper polariton branches to the lowest one (53).

For the lower concentration β-carotene sample we were able to reliably resolve three hybrid branches in D1 geometry, i.e., energy splittings corresponding to the strong coupling between SPP and the β-carotene transitions (0-0) and (0-1) (see Fig. 3.2 (b)). Fig. 3.8 illustrates the experimental finding together with the reflectance coefficient calculated by utilizing the transfer matrix method. Experimental dispersion relations together with the fits by the coupled oscillators model are shown in Fig. 3.9. In D1 the 0-0 and 0-1 splits are 80 and 130 meV, correspondingly, while the D2 data yield 120 meV for the 0-0 gap. The 0-1 gap was not resolvable in D2. The concentration study presented in inset of Fig. 3.8 shows that we deal with strong coupling interaction.

In principle, in order to observe the strong coupling phenomena the strength of the coupling should be greater than a sum of the half-widths of the absorption resonance and surface plasmon polariton resonance. It holds for the case of the studied

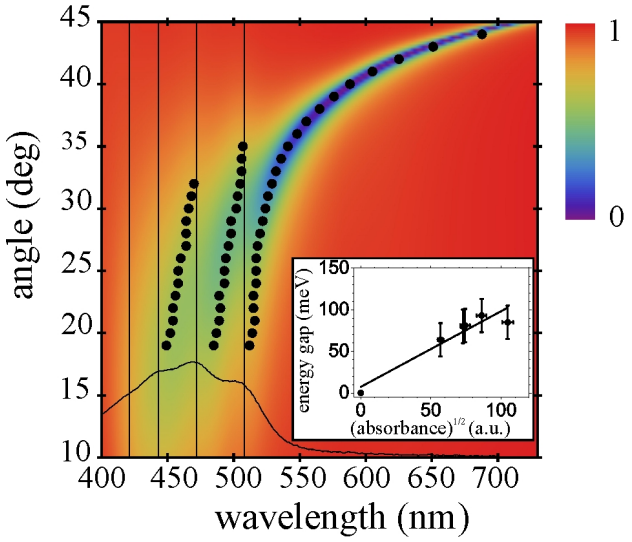

FIGURE 3.8 Calculated reflectance coefficient as a function of the excitation wavelength and angle $90° - \alpha$ (color scale) together with the measured minima of the reflected light spectra, D1 (black circles). Black curve is the measured absorption spectrum of the same β-carotene thin film but without silver, and the vertical black lines indicate positions of its maxima. The inset represents the dependence of the width of the lowest energy gap on a square root of the total absorbance of the β-carotene film together with its linear fit. Adapted from the paper **II** of the thesis.

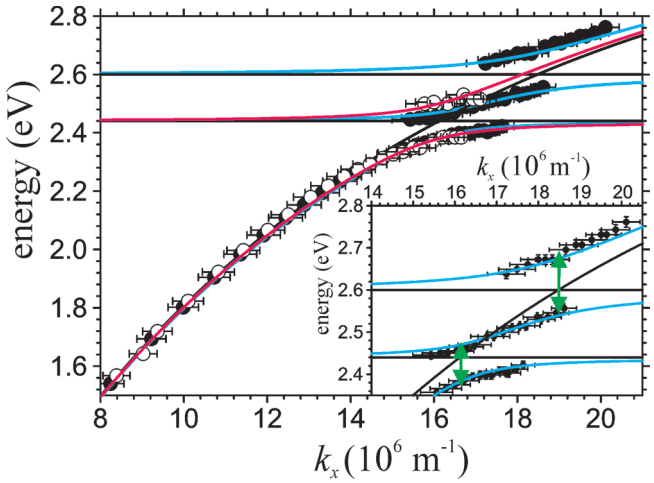

FIGURE 3.9 The dispersion curves obtained in D1 (black circles) and D2 (empty circles). Black horizontal lines represent the two lowest absorption maxima of β-carotene, i.e., (0-0) and (0-1); black curve is the SPP dispersion relation of a sample without β-carotene. Blue and pink curves are results from the coupled oscillator model fitted to the D1 and D2 data, respectively. Inset shows the zoomed gap regions of the D1 dispersion relation. Adopted from the paper II of the thesis.

silver-SR101 system. The absorption half-width of 1 mg SR101 sample is 66 meV, and the half-width of SPP resonance in silver-SU8 structure is 100 meV at the energy which is close to main molecular absorption maximum. The sum of these values is lower than the observed 200 meV splitting. In addition, we have to take into account that the strong coupling condition assumes the linewidths being only due to lifetime broadening, which makes it possibly to state the condition in other way: in strong coupling regime the period of the Rabi oscillation have to be shorter than the sum of the decay times of the components. In our case the broadening of the molecular absorption is mostly due to molecule's vibrational states and conformational diversity due to environment. The γ due to lifetime broadening can be much smaller, thus fulfilling the equation 2.20 and the above time resolved condition. Thus, we assume as in (80) that the system is in strong coupling regime when the Rabi split is resolved in measurement.

3.2 Possible routes of energy transfer

Unlike in earlier experiments (7; 79) we also detect emission of the upper polariton branch, however, this is much weaker than that from the lower branches at all angles (Fig.3.10 (b)). According to Moreland et.al. (61) the efficiency of the SPP to photon conversion for rough silver film of 50 nm thickness is around 6%. Very similar behavior has been reported from photoluminescence of microcavities containing J-aggregates (53). It was proposed that a population transfer from the upper to the lower branches occurs by the emission of energy in the form of vibrational quanta (21). The rate-equation model describing the population, depopulation and transfer between polariton and excitation states is elaborated in (22) for the case of cavity containing excitation states that belong to two different sort of molecules. A simpler model that includes the energy transfer between polaritonic modes is presented in (53). In mentioned cavity studies the excitation reservoir is pumped by laser light and then scattering to the polariton branches occurs. Interbranch transition and radiative decay of polaritons can take place. In this model the intensity of the branches can be calculated using formula

$$I_u(\theta) = \frac{\Phi U_u(\omega)\beta_u^2}{1 + \rho(\theta)\tau_{cav}\alpha_u^{-2}}, \tag{3.4}$$

$$I_l(\theta) = \Phi\left(\frac{U_l(\omega)\beta_u^2}{1 + \rho^{-1}(\theta)\tau_{cav}^{-1}\alpha_u^2} + U_l(\omega)\beta_l^2\right), \tag{3.5}$$

where Φ is a scaling coefficient, $U_{u,l}$ is a relative number of uncoupled excitations having enough energy to scatter into a particular state. α_u and $\beta_{u,l}$ are the coefficients of the cavity photon (or it can be also SPP) and excitation deduced from the coupled

oscillators model. τ_{cav} is the escape time of an uncoupled photon from the cavity and the transition rate between the branches $\rho(\theta) = K_{u-l}\beta_u^2\beta_l^2$, where K_{u-l} is a rate constant.

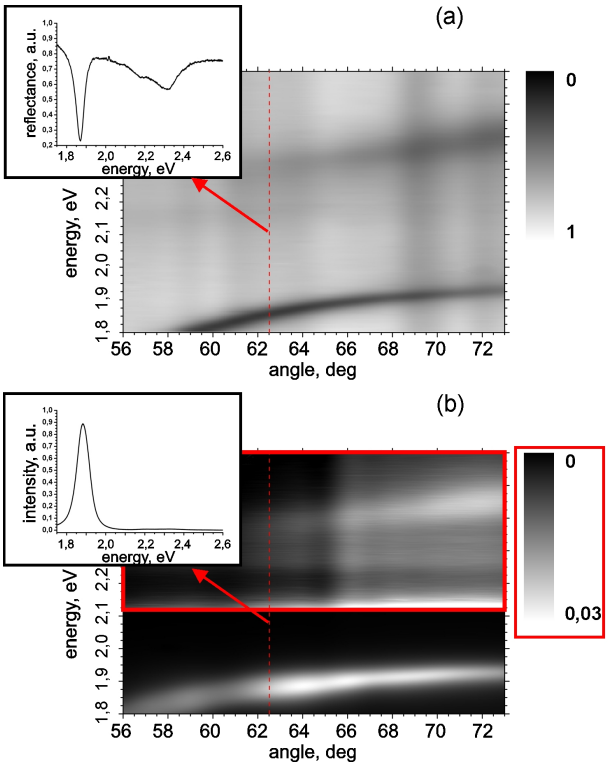

FIGURE 3.10 (a) Measured reflectance, (b) measured scattered radiation as a function of the excitation energy and the angle for silver/SR101 2 mg sample. Adapted from the paper **I** of the thesis.

Unfortunately, this model does not give reasonable results when applied directly to a SPP case. In (22) it is shown that the middle polariton branch acts as a channel for the higher energy excitation relaxation to the lower energy excitation from where the lower branch is populated.

The strong coupling regime does not forbid the intramolecule vibrational relaxation, which can cause low quantum yields of emission. Also fast vibrational transitions are responsible for upper state decay to lower polaritonic state or uncoupled molecular states. In (20) it is shown that population of lower polaritonic state close to $k_{||} = 0$ is due to the decay of upper and lower polaritonic components that have small photonic component.

Recently the absence of mutual scattering among strongly coupled SPP - molecular excitation modes was shown for Nile Red dye that have a very large Stokes shift (50). Authors prove that the polaritons decay to molecular excitations via internal relaxation of the molecules. In (34) the nature of the lower polariton branch emission of molecules coupled to an optical cavity was investigated by means of excitation spectroscopy and transient absorption measurements. Authors found out that all

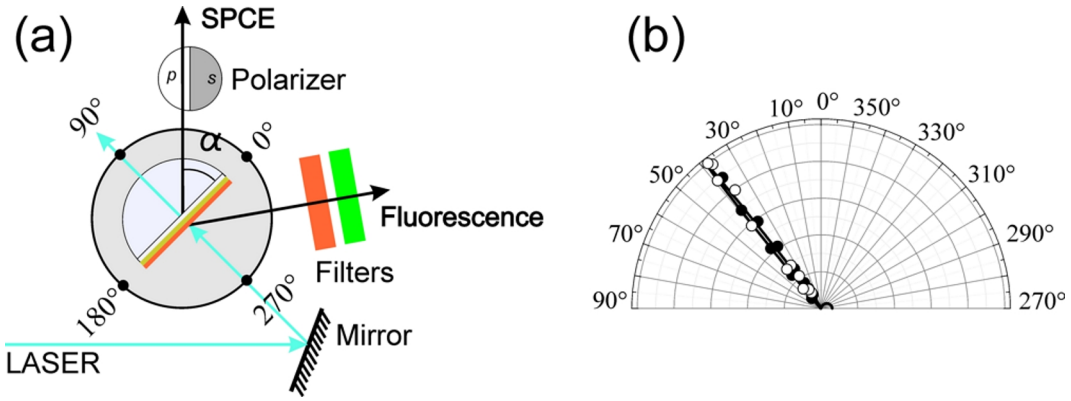

FIGURE 3.11 (a) Schematic representation of the experimental setup for the SPCE observation. (b) Measured radiation profiles for an emission at 570 nm excited with 488 and 514 nm (empty and black circles, correspondingly). Solid line is the calculated profile. α is the detection angle. Adapted from the paper **II** of the thesis.

the lower branch emission is due to the excitation of the upper polaritonic branch. They suggested that the relaxation to the lower polaritonic states happened via internal vibrational relaxation. However, this study raised the question what was the origin of strong static absorption of the lower polaritonic branch.

3.3 Surface plasmon coupled emission and SERS

In order to perform this part of the study, the setup was slightly modified to the configuration shown in Fig. 3.11 (a) . The samples were excited from the molecule side with 488 or 514 nm lines of Stelar-Pro multi-line argon laser (Modu-Lasers), and the emission was collected from the prism side as well as from the molecule side. This method of excitation is often referred to as a reverse Kretschmann configuration (35).

Collecting of surface plasmon coupled emission (SPCE) from the prism side is another way to obtain a part of the dispersion relation since we can now scan the detection angle, α, and register the emission energy on that direction. From these the wavevector can be extracted straightforwardly. We used 514 and 488 nm laser lines for the excitation of SR101 and β-carotene excitation, correspondingly. As seen from the Fig. 3.12 the obtained SPCE overlaps nicely with the fluorescence of the molecules and with lower dispersion branch.

In $0° - 90°$ region we observe a strongly directed emission at 38° that is the SPCE. In case of the most concentrated β-carotene sample, the SPCE spectrum shows additional peaks (Fig.3.13). We assigned those peaks to β-carotene Raman active vibrations $v_1 = 1525$ cm^{-1}, $v_2 = 1155$ cm^{-1}, $v_3 = 1005$ cm^{-1} and their combinations $2v_1$, $2v_2$, and $v_1 + v_2$ according to Ref. (40). Those peaks are not the fluorescent peaks with different vibrationally excited final states. According to "mirror image rule" the

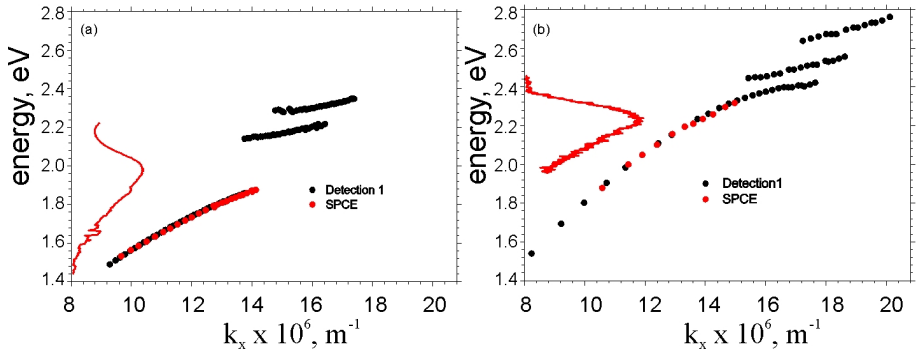

FIGURE 3.12 (a) SPCE of SR101 excited with 514 nm laser (red circles) together with the D1 dispersion measured from the same sample (black circles). Solid red curve is the fluorescence of the 50 nm thick SR101/SU-8 layer deposited on the silver. (b) SPCE of β-carotene excited with 488 nm laser (red circles) together with the D1 dispersion measured from the same sample (black circles). Solid red curve is fluorescence of 40 nm β-carotene on silver.

distance (in terms of wavelength) between those peaks must be the same as the distance between peaks in absorption spectrum. Next the detector was equipped with a polarizer and the sample emission polarization was also tested with all the angles. Fig. 3.13 (b) shows the presence of the same sharp Raman peaks in $270° - 360°$ region regardless of the detected polarization, while only the p-polarized peaks were observed in the $0° - 90°$ region as shown in Fig. 3.13 (a). The absence of the s-polarized signal in this region and the intensity dependency of the peaks on the detection angle proves that the Raman scattered radiation was coupled to SPPs and mediated by them, and not appearing at the prism side due to interaction with a possibly leaking laser radiation.

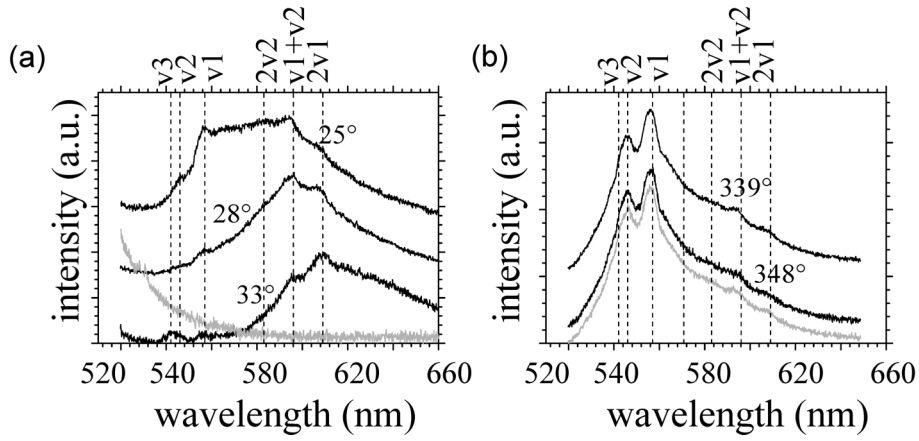

FIGURE 3.13 Measured p-polarized SPP coupled Raman signals at several detection angles (black curves) and corresponding s-polarized signal (gray curve) with 514 nm excitation at (a) SPCE and (b) fluorescence regions. The dashed lines indicate positions of the Raman shifted bands. In all the images the spectra have been offset for clarity. Adapted from the paper II of the thesis.

In (23; 81) the Kretschmann prism coupling configuration is used to excite SPP at the laser frequency and to couple out the Raman shifted SPP. The angular position of the scattered signal is governed by SPP's dispersion relation. In our case of reverse Kretschmann configuration it is natural to adopt mechanism similar to the SPCE generation. Namely, the initial far field excitation is directly exciting the molecules (resonantly or virtually) and the subsequent emission to another vibrational state inducing the Raman shift, is coupled to SPPs via its near-field. Then SPP travels along the metal surface before it scatters to the photons that are detected.

Chapter 4

Scattering analysis of the SPP-molecular excitation -polariton

We experimentally demonstrate polarization conversion of scattered SPPs. It is assigned rather to the properties of strongly coupled molecular state than to surface plasmon polariton scattering on metallic film imperfections. The theoretical model based on relation of SPP and molecular excitation relative weight is elaborated. The experimental findings indicate that the samples with molecules with larger Stokes shift show less TE polarized intensity.

4.1 Modified coupled oscillator model

In this part we introduce an extension into the coupled oscillator model. Instead of fitting the coupling strength parameters as discussed in Section 2.3, we consider coupling strength between individual oscillator, i.e. j^{th} molecular excitation, and SPP field

$$g_j(k_x) = \sqrt{\frac{\omega(k_x)}{2\epsilon_0 L(k_x)}} e^{-k_z z} \vec{\mu_j} \cdot (\hat{u}_x + i\frac{k_x}{k_z}\hat{u}_z), \tag{4.1}$$

where $\omega(k_x)$ is the SPP dispersion relation, $L(k_x)$ is an effective length of the mode calculated using relation in (3), ϵ_0 is vacuum permittivity and index *j* refers to a type of molecule with excitation energy E_{Exj} and the molecular dipole moment of $\vec{\mu} = \mu\hat{u_j}$. The term $\hat{u}_x + i\frac{k_x}{k_z}\hat{u}_z = \hat{u}_p$ is the SPP polarization vector with $k_z = \sqrt{k_x^2 - \frac{\omega^2}{c^2}}$.

To take into account all the molecules we have to sum over their coupling strengths. If we assume homogeneous distribution of molecules with randomly oriented dipole moments, we can transform the sum into integrals over z and the angle, ϕ, between the dipole $\vec{\mu}$ and the direction of plasmon electric field $\hat{u}_p$. Assuming two different kind of molecules with energies E_{Ex1} and E_{Ex2}, densities n_1 and n_2, dipole

moments μ_1 and μ_2, and thus couplings $g_1(k_x)$ and $g_2(k_x)$, we can write the equation for the previous coupled oscillator model as

$$\begin{pmatrix} E_{SPP}(k_x) & G_1(k_x) & G_2(k_x) \\ G_1(k_x) & E_{Ex1} & 0 \\ G_2(k_x) & 0 & E_{Ex2} \end{pmatrix} \begin{pmatrix} \alpha \\ \beta \\ \gamma \end{pmatrix} = \epsilon \begin{pmatrix} \alpha \\ \beta \\ \gamma \end{pmatrix}, \tag{4.2}$$

where $G_j(k_x) = \sqrt{n_j \int_0^D \int_0^{2\pi} |g_j(k_x, z)|^2 d\phi dz}, j = 1, 2$, D is thickness of the resist layer. Note that due to the random orientation of the molecules within the resist the fitted transition dipoles have an effective values averaged over the all orientations.

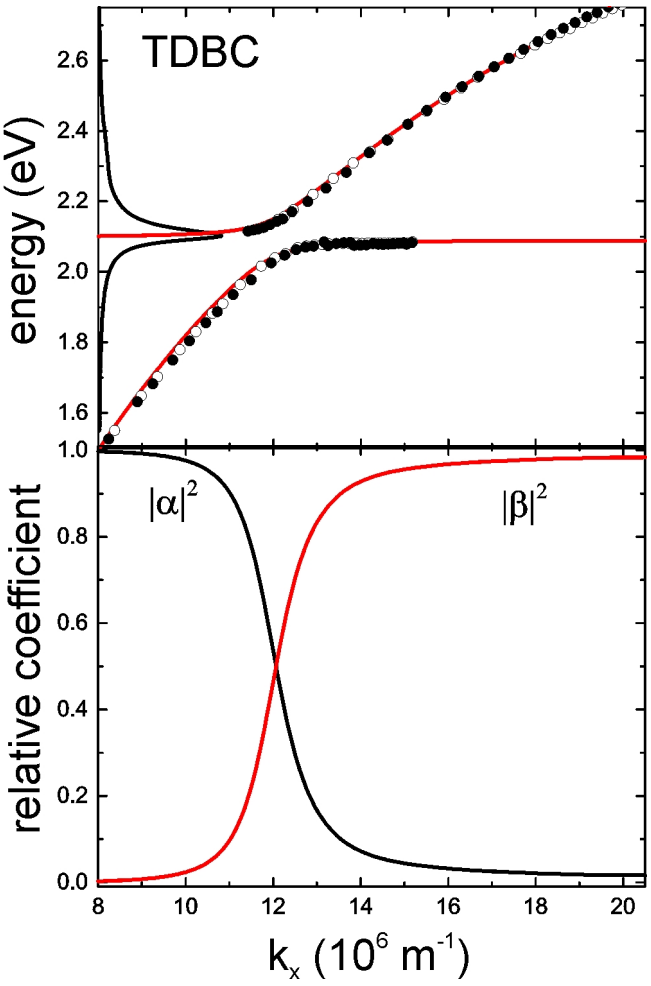

FIGURE 4.1 Upper panel shows dispersion curve for a TDBC sample (black circles) fited by extended coupled oscillator model (red solid line). Absorbance of the reference TDBC sample is shown as black solid line. Lower panel shows relative weights of the lower polariton branch. Adapted from the paper **IV** of the thesis.

As an example we consider a TDBC sample dispersion relation fitted with coupled oscillators model (Fig. 4.1). Now there is only one type of molecules, i.e.

$j = 1$, and $\mu_1\sqrt{n_1}$ is used as the fitting parameter. The best fit is achieved with $\mu_1\sqrt{n_1} = 3.4 \times 10^{-16}$ Cm$^{-1/2}$. If one assumes effective transition dipole moment to be 32 D (33) one obtains $n_1 = 10^{25}$ m^{-3}. This is one order of magnitude higher than the molecule concentration in the initial solution, which makes sense since in thin film we have higher concentration due to solvent evaporation.

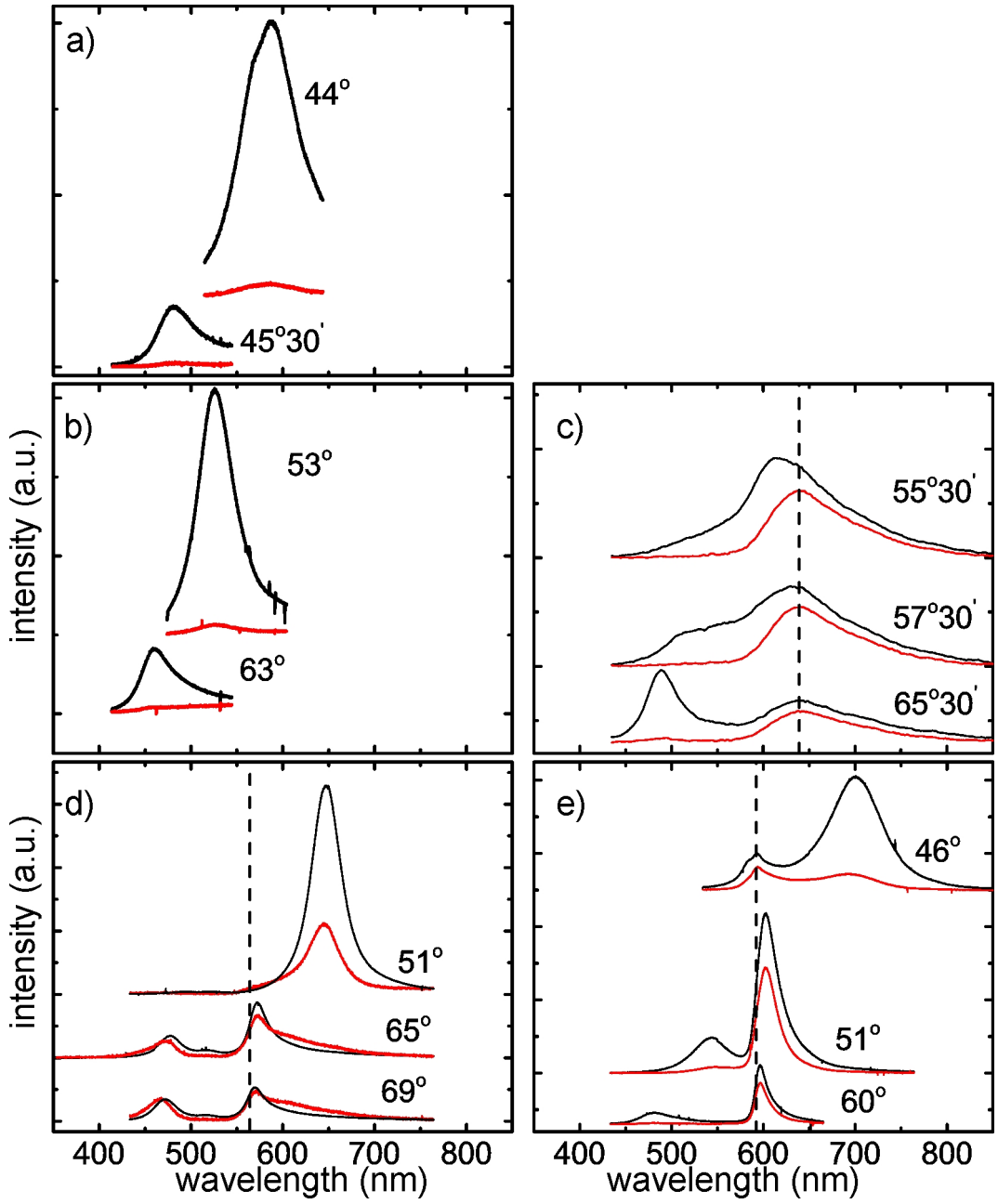

FIGURE 4.2 Detection 2 spectra of (a) silver, (b) silver-SU8, (c) silver-NR, (d) silver-R6G and (e) silver-TDBC samples. Black curves are TM polarized signals; red curves are TE polarized signals. TE polarized intensity of silver-R6G sample is increased in 10 times. The curves are shifted vertically for clarity. Dashed line indicates the position of the fluorescence peak of the molecule. Adapted from the paper **IV** of the thesis.

Lower panel on Fig. 4.1 shows relative weights α and β for the lower TDBC-plasmon branch. It is worth to note that molecules are considered as single oscillator and β coefficient has effective value. The more precise treatment requires considering individual molecule couplings with SPP field. In this case the matrix that describes the interaction becomes $(N+2)(N+2)$ matrix. Except two states that describe lower or upper polariton branches one gets $N-1$ eigenstates that include only molecular excitations. This also means that molecular excitations become delocalized, which have consequences for increasing exciton and electrical conductance as proven in (29; 67).

4.2 Effect of Stokes shift on polarization of the emission of SPP-molecular excitation -polariton

4.2.1 Experimental results

The fundamental property of SPP in planar silver-dielectric structures is its pure TM (p) polarization. However, it was observed that in the case of metal-air interface the SPP scattered radiation can have both polarizations depending on the observation direction (10), (12). But still the comprehensive treatment of this phenomenon is missing from literature. As control experiments we performed SPP emission measurements for two polarizations for 50 nm thick silver film and 50 nm silver/50 nm SU-8 resist samples. In both cases only TM polarized radiation was observed (Fig. 4.2 (a), (b)). But the situation changed when we proceeded to the samples having fluorescent dye within the resist layers. We tested three fluorescent dyes that have different Stokes shifts. As can be seen from Fig. 4.2, in the case of Nile Red (NR) dye, that has the highest Stokes shift (350 meV), there is no TE polarized signal detected from the polariton scattered emission. Only TE polarized emission that was visible comes from the fluorescence of the molecule. But as we changed to the molecules with lower Stokes shift - R6G (Stokes shift 90 meV) and TDBC (Stokes shift is practically zero) - we were able to measure polariton signal of both TM and TE polarizations. Besides polariton scattering peak we always detected fluorescence of the molecules. Fluorescence peak did not move when the angle of excitation was changed. The fluorescence is unpolarized thus contributing to both TM and TE spectra.

4.2.2 Theoretical approach to emission problem

We considered a ratio between the TM and TE emission signals of different polariton branches and plotted it on Fig. 4.3 for several samples. In order to get the total intensity at certain wave vector we integrated the intensity spectrum with respect

to wavelength separately for lower and upper branches. We did not distinguish between polariton scattered intensity and fluorescence as they have the same polariton origin (50).

For the lower dispersion branch the TM to TE ratio is higher in the region of small wavevectors, where SPP-molecule excitation hybrid state is mostly plasmonic (Fig. 2.6 and 4.1). But it decreases towards the gap region where the hybrid state has more molecular state properties. One could expect that for the upper branch the behavior would be the same - the growth of the ratio with increasing wavevector as the dependence of the coefficients $|\alpha|^2$ and $|\beta|^2$ go other way around. However, in case of R6G we are not able to observe such dependence. Also in the case of TDBC the behavior shows only a weak growth.

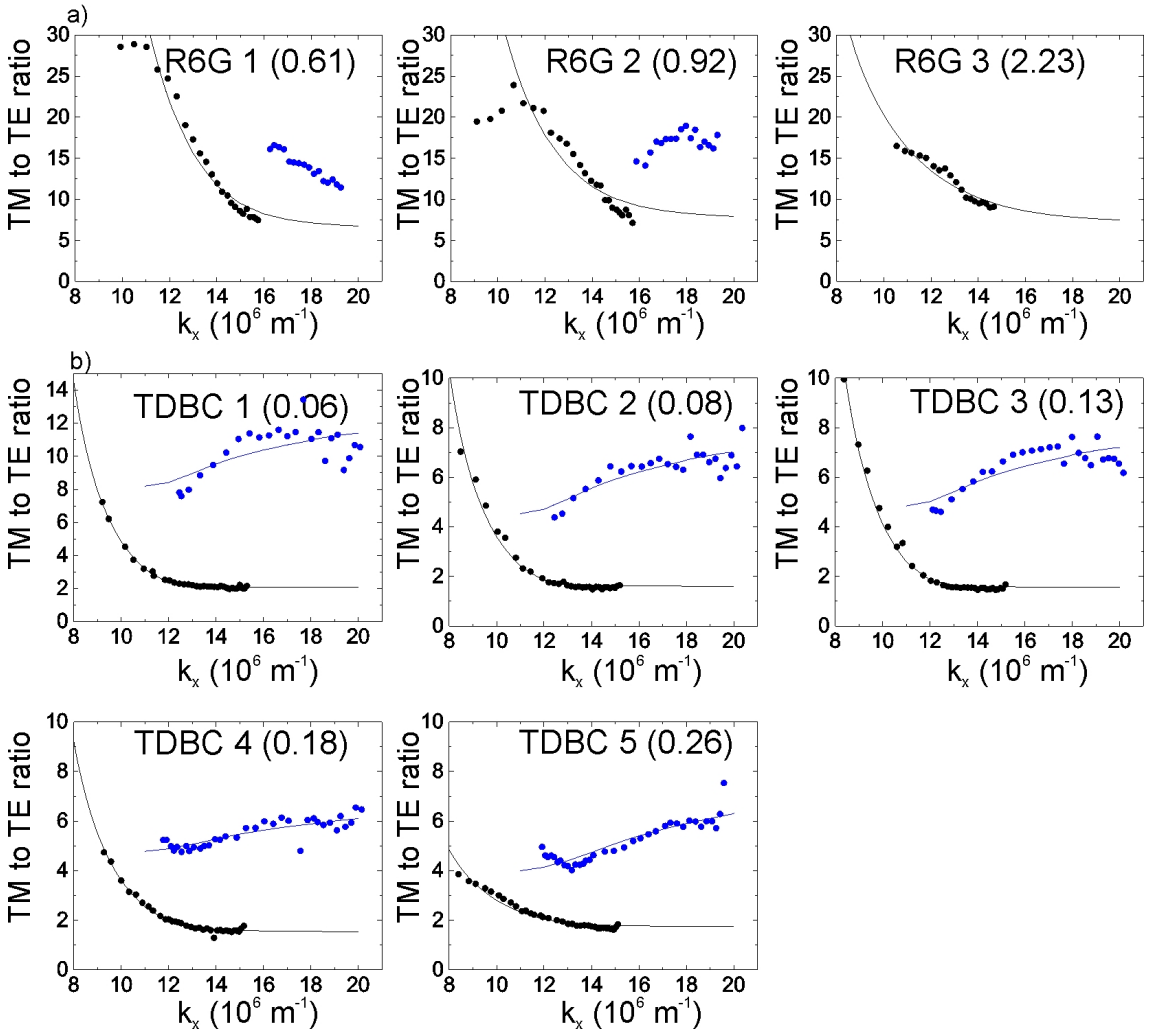

FIGURE 4.3 Ratios of TM to TE signal intensity for R6G samples (a) and TDBC samples (b). Experimental ratio of lower branch illustrated as black dots and upper branch as blue dots. Solid black line and blue line are theoretical fits. Sample names are presented in brackets. They indicate molecule/photo resist mass ratio. Adapted from the paper **IV** of the thesis.

In order to estimate the ratio between TM and TE emission we compare radiation decay rates of SPP-molecule polariton calculated with the help of Fermi's Golden rule

$$\frac{\Gamma^{TM}_{i\to f}}{\Gamma^{TE}_{i\to f}} = \frac{|\langle \Psi_f | H^{TM}_{int} | \Psi_i \rangle|^2}{|\langle \Psi_f | H^{TE}_{int} | \Psi_i \rangle|^2}. \tag{4.3}$$

Total Hamiltonian of interaction between SPP-molecule polariton and a photon, i.e. Hamiltonian describing the scattering of the polariton to a photon, is described as following within the fully extended basis treating coupling of each molecule separately

$$\begin{aligned} H^{TM/TE}_{int} = g^{TM}_{SPP}(\hat{u}_p \cdot \hat{u}_x)(a^\dagger c_{TM} + c^\dagger_{TM} a) + \sum_{j=1}^{n} [g^{TM}_m (\hat{u}_j \cdot \hat{u}_x)(b^\dagger_j c_{TM} + c^\dagger_{TM} b_j) + \\ g^{TE}_m (\hat{u}_j \cdot \hat{u}_y)(b^\dagger_j c_{TE} + c^\dagger_{TE} b_j)], \end{aligned} \tag{4.4}$$

where $a^\dagger$ and a are the creation and annihilation operators of SPP, $b^\dagger_j$ and b_j are the creation and annihilation operators of excitation of j^{th} molecule, $c^\dagger$ and c are the creation and annihilation operators of a photon. Coupling strengths g^{TM}_{SPP} and $g^{TM/TE}_m$describe the coupling between the SPP and a photon of given polarization, and between a molecular excitation and a photon, respectively. $\hat{u}_p$ is again the polarization unit vector of SPP and $\hat{u}_j$ is the polarization unit vector of j^{th} molecule.

The final state corresponds to the case where one photon is created, $\Psi_f = c^\dagger|0\rangle$. Here $|0\rangle$ describes a vacuum state , *i.e.*, no SPP nor any molecular excitations present. The initial state wave functions of lower (L) or upper (U) branch can be written as

$$\Psi_i = \alpha^{L/U}(k_x) a^\dagger_{k_x} |0\rangle + \sum_j \beta^{L/U}_j (k_x) b^\dagger_j |0\rangle, \tag{4.5}$$

here $\alpha^{L/U}(k_x)$ and $\beta^{L/U}_j(k_x)$ describe the fraction of SPP and excitation on j^{th} molecule in the polaritonic state. It is worth to emphasize that we are not dealing with uncoupled molecules and SPP, but considering the coupled hybrid state between SPP and many molecules. In order to derive these coefficients we treat the total Hamiltonian of interacting SPP and molecules , *i.e.*, the extended coupled oscillator model, in the same way as it is done in Ref. (1) for an interacting cavity mode and molecular excitations. Assuming that all the molecules are of the same type, *i.e.*, have the same excitation energy, E_0, and density n_0 the Hamiltonian can be written in the form

$$H = E_{SPP} a^\dagger a + \sum_j E_0 b^\dagger_j b_j + \sum_j g_j(k_x)(a b^\dagger_j + a^\dagger b_j), \tag{4.6}$$

where E_{SPP} is the SPP energy, $g_j(k_x)$ is the coupling between molecular excitation and SPP and it is described by equation 4.1 except that now *j* refers to a j^{th} molecule and not to the type of the molecule. Following the reasoning in Ref. (1) we introduce new Bose operators

$$\xi^\dagger = \alpha a + \sum_j \beta_j b_j^\dagger,\ \xi = \alpha^* a^\dagger + \sum_j \beta^* b_j. \tag{4.7}$$

After the substitution and solving the eigenvalue problem, it is found that coefficients are connected via following system of equations

$$\begin{aligned} \alpha(E - E_{SPP}) &= \sum_j g_j(k_x)\beta_j, \\ \beta_j(E - E_0) &= g_j(k_x)\alpha. \end{aligned} \tag{4.8}$$

Also, we use the normalization condition $|\alpha|^2 + \sum_j |\beta_j|^2 = 1$ to derive the coefficients. Finally, we obtain following expressions for the coefficients

$$|\alpha^{L/U}(k_x)|^2 = \frac{(E^{L/U}(k_x) - E_0)^2}{(E^{L/U}(k_x) - E_0)^2 + G_0^2}, \tag{4.9}$$

$$|\beta_j^{L/U}(k_x)|^2 = \frac{G_0^2}{(E^{L/U}(k_x) - E_0)^2 + G_0^2}, \tag{4.10}$$

where $E^{L/U}(k_x)$ is dispersion relation of the lower/upper SPP-molecule polariton branch, G_0 is defined earlier and it is dependent on the density of molecular excitations with energy E_0 and dipole moment.

After substitution of equations 4.4 and 4.5 into 4.3 one gets following relation for the ratio of the decay rates

$$\frac{\Gamma_{i\to f}^{TM}}{\Gamma_{i\to f}^{TE}} = \frac{|g_{SPP}^{TM}(\hat{u}_p \cdot \hat{u}_x)\alpha^{L/U} + g_m^{TM}\sum_j(\hat{u}_j \cdot \hat{u}_x)\beta_j^{L/U}|^2}{|g_m^{TE}\sum_j(\hat{u}_j \cdot \hat{u}_y)\beta_j^{L/U}|^2}. \tag{4.11}$$

In our case dipoles have equal absolute value of transition dipole moment but random orientation in space. If we consider the TE transition/emission probability which is

$$\Gamma_{i\to f}^{TE} = \left| g_m^{TE}\sum_j(\hat{u}_j \cdot \hat{u}_y)\beta_j^{L/U} \right|^2 \propto \left| \sum_j(\hat{u}_j \cdot (\hat{u_x} + i\frac{k_x}{k_z}\hat{u}_z))(\hat{u}_j \cdot \hat{u}_y) \right|^2, \tag{4.12}$$

we get zero after summing up of all the scalar products. However, this contradicts the experimental observation. Since the above description assumed fully coherent state, the TE polarized emission observed in the experiments should be due to a decoherence in the system which would revoke the treatment above. This is a reasonable assumption as the decoherence is usually high in systems with to many molecular degrees of freedom at room temperature. Also it can be that transition dipole moments in our system are not fully randomly oriented. In order to deal with this contradiction we assume that the superposition state has time to undergo dephasing before the emission of a photon, *i.e.*, dephasing rate is faster that the emission rate. This means that we can associate the molecules that interacts with SPP field with a total dipole moment similarly as we do in case of coupled oscillators model.

As previously the coefficients $\alpha^{L/U}(k_x)$ and $\beta^{L/U}(k_x)$ are real numbers when the final widths of SPP and molecular transition are neglected. Now instead of $\sum_j \beta_j^{L/U}$ we have single $\beta^{L/U}$. And the multiple molecules problem is reduced to the previous coupled oscillators problem (see Eq. 4.2).

To obtain the final expression for the rate ratio that is used in fitting, one has to substitute $\alpha^{L/U}$ with equation 4.9 and calculate $\beta^{L/U}$ using the normalization condition. Finally one gets

$$\frac{\Gamma_{i\to f}^{TM}}{\Gamma_{i\to f}^{TE}} = \left| \frac{g_m^{TM}}{g_m^{TE}} + \frac{g_{SPP}^{TM}}{g_m^{TE}} \frac{E^{L/U}(k_x) - E}{G(k_x)} \right|^2 . \tag{4.13}$$

In this calculation we included values of the unit vectors scalar products into $g_{m,SPP}^{TE,TM}$. We use ratios g_m^{TM}/g_m^{TE} and g_{SPP}^{TM}/g_m^{TE} as fitting parameters to obtain the curves plotted on Fig. 4.3. For example for TDBC sample 3 (0.13) we have a reasonable fit for lower energy branch with $g_m^{TM}/g_m^{TE} = 1.233$ and $g_{SPP}^{TM}/g_m^{TE} = 0.124$. The fitting parameters for the rest of the samples can be found in Table 4.1. Ratio g_m^{TM}/g_m^{TE} deviates from unity which means that the emitted field has more TM component. This ratio defines the ratio of TM to TE emission in case when coefficient α goes to zero (the second term in equation 4.13 vanishes), which is true at high wavevectors for the lower polariton branch. But still in this region we have coupling to SPPs even though the nature of coupled state is molecular. Most likely in the region of high wavevectors we deal with SPP scattered signal together with unpolarized fluorescence. As a result TM to TE intensity ratio is higher than unity.

In this model we have a single dipole that has certain orientation with respect to the SPP field. The electromagnetic field that is emitted by the dipole is linearly polarized and direction of electric field is defined by dipole orientation in space. Thus the ratio g_{SPP}^{TM}/g_m^{TE} depends on the dipole orientation very strongly. In current calculation we assume that $\mu_x^2 = \mu_y^2 = \mu_z^2 = \frac{1}{3}\mu^2$ corresponding to random orientation of molecules, which we wanted to model.

In the case of TDBC it is not possible to fit the upper branch TM to TE ratio

with the parameters g_m^{TM}/g_m^{TE} and g_{SPP}^{TM}/g_m^{TE} that were obtained in the lower branch fitting. The ratio is higher than predicted one. We can speculate that the intensity redistribution occurs between coupled state and uncoupled molecules. For example, the amount of TE intensity gets smaller due to its transfer to uncoupled molecules.

For R6G samples we cannot get a good fit with suggested model even though the TM to TE ratio dependence on wave vector is qualitatively correct. Also, in the region of maximal wave vectors the ratio is much greater than unity. The possible reason for model failure is that it does not count for relaxation dynamics of the molecules.

TABLE 4.1 Fitting parameters of TM to TE signal intensity ratios of the lower branch

Sample	g_m^{TM}/g_m^{TE}	g_{SPP}^{TM}/g_m^{TE}
1. R6G 0.61	2.384	0.527
2. R6G 0.92	2.586	0.476
3. R6G 2.23	2.570	0.287
1. TDBC 0.06	1.426	0.105
2. TDBC 0.08	1.255	0.097
3. TDBC 0.13	1.233	0.124
4. TDBC 0.18	1.211	0.144
5. TDBC 0.26	1.303	0.078

We observe that samples that have molecules with different Stokes shifts between absorbance maximum and fluorescence show different TM to TE signal polarization ratio in general. The employment of Nile Red molecule which has very high Stokes shift (350 meV) leads to a situation where TE polarized signal is completely absent (50). When Stokes shift decreases from 90 meV for R6G to practically zero for TDBC, TM to TE polarization ratio decreases from 30 to 6 for the lower polariton branch with wavevector component around 9.3×10^6 m^{-1}. We can gain more insight into this phenomenon taking into account that Stokes shift is proportional to the energy difference between the Franck-Condon region and the minimum of the electronic excited state potential energy surface. The larger this difference, the higher the gradient of potential energy, and the rate with which the molecule reaches excited state minimum. This implies that molecules with higher Stokes shift will decay faster, thus implying that they do not have time to dephase before emission of the photon. Due to this more emission comes from a coherent state and thus with only TM polarization as discussed above.

In the case of Nile Red, polaritons decay very fast to molecular fluorescent state producing fluorescence that is unpolarized. Due to their high decay rate polaritons do not have time to dephase and all the polariton emission originate from a coherent state and is thus purely TM oriented. In case of R6G which has smaller Stokes shift the molecular component decay time is longer, meaning that SPP-molecular excitation hybrid have more time for dephasing and thus to produce the TE emission.

The relaxation associated with Stokes shift thus competes with dephasing, which leads to different values of TM to TE ratio depending on the Stokes shift. TDBC has the smallest Stokes shift and correspondingly the longest molecular excitation decay time. It is thus more probable for it to dephase fully and thus emit more TE polarized emission.

Thus, in order to gain more understanding of appearance of TE polarized signal the interplay between the dephasing time and the decay time of molecule into its fluorescing state has to be considered. For molecules with larger Stokes shift the decay rate is faster than dephasing rate. Thus the polariton emission originates from a coherent state and it is TM polarized. The absence of TE polarized emission in case of coherent state is due to destructive interference between TE polarized radiation emitted by dipoles. But once the Stokes shift gets smaller and decay rate slower the dephasing start to be significant and molecules start to emit unpolarized radiation as discussed above. The presence of some amount of destructive interference even the dephasing would be dominating, can lead to reduced TE polarized emission in case of molecular-like polaritons for R6G and TDBC ($g_m^{TM}/g_m^{TE} > 1$).

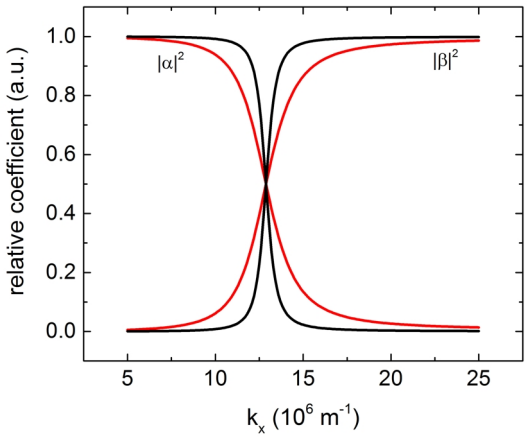

FIGURE 4.4 Relative coefficients for a model system with coupling strength 30 meV (black curve) and 90 meV (red curve).

This also explains the previous result in the case of molecule with high Stokes shift (Nile Red) that the fluorescence intensity can be described purely by the polariton coefficients in form of $\sum_n \alpha_n^2(\beta_n^2 + \gamma_n^2)$ (where n labels lower, upper and middle branch). Coefficients α_n, β_n and γ_n are calculated from coupled oscillators model. This is further strengthened by showing that excitation of upper SPP branch by 488 nm laser does not lead to appearance of lower branch polaritons. Only fluorescence signal was observed, meaning that there is only relaxation to molecular excitation state (50).

Examination of Fig. 4.3 shows that there is concentration dependence of TM to TE ratio. The general rule is the higher the concentration the smaller the ratio.

The tendency to have more TE intensity in higher concentration samples at lower wavevectors can be explained by higher molecular coefficient $|\beta|^2$ for system with higher coupling strength as illustrated on Fig. 4.4.

Chapter 5

Summary and perspectives

In article **I** strong coupling between SPPs and SR101 dyes in the planar silver-SR101 resin structures was demonstrated by using two complementary detection geometries. Double Rabi splitting was observed with energies up to 360 and 190 meV. Both, the transfer matrix method and the coupled oscillator models fit the experimental data nicely, and the energies of the observed Rabi splittings depend linearly on the square root of the oscillator strength proving the coherent strong coupling between the SPP and the dye molecules. The employed scattered radiation measurements (D2) allowed us gaining some insight into the dynamics of the SPP-molecule interaction. The lower energy gap values obtained by the D2 measurements was larger, which is consistent with the earlier observations and means that the interaction time between the propagating SPP and molecules is longer than the one allowed within the time frame of the reflectance measurement, where exciting photon immediately leaves the active volume, thus reducing lifetime. However, the upper energy split is most probably influenced by a strong decrease of the SPP lifetime leading to a decrease of the Rabi energy in D2. However, as the splits are not fully separate, but coupled via shared middle branch, no exact conclusion can be drawn. On the other hand, the intensity of the upper polariton branches was reduced in D2 compared to D1 much more in the case of SR101 than with other molecules, hinting about reduced lifetime of them.

In article **II** the strong coupling of SPPs to the two lowest vibrational bands of the S_2 state of the β-carotene is observed with coupling energies up to 130 meV. A strong surface plasmon coupled emission, together with a surface enhanced and SPP coupled Raman signals were detected. The Raman signal was found to get more dominant over the fluorescence with increased β-carotene concentration. This measurements also clearly clarifies that the different vibrational states can couple separately to the SPPs.

In article **III** we analyze fluorescence that appears due to decay of the excited SPP-molecular hybrid state into molecular excitation and its further relaxation to a fluorescing state. In earlier study it was shown that this decay to molecular fluores-

cence happens faster than any mutual polariton scatterings in the case of Nile Red. In this study we obtained suggestions that the same could hold for SR101, which would explain also the reduced polariton lifetime suggested in article **I**.

In article **IV** we report on behavior of emission of SPP-molecule polaritons in samples containing different dye molecules. We assign the presence of the observed TE radiation rather to the molecular properties of the strongly coupled hybrid state than to SPP scattering on metallic film imperfections, which was shown to have only TM polarization. The ratio TM/TE for the emitted polariton radiation decreases when the SPP-molecular hybrid state is approaching the energy gap region. The theoretical model that describes wavevector dependence of TM to TE scattered intensity ratio is elaborated and it shows that in addition to the molecular contribution of the hybrid state also decoherence is needed for the TE polarized emission to appear. Assuming some decoherence the wavevector dependency of the modeled TM/TE ratio agrees well with the measurements on molecules with negligible Stokes shift, *i.e.* TDBC. However, the molecules with higher Stokes shift do not agree so well. The measurements actually suggest that the higher is the Stokes shift the less TE polarized emission is detected. The extreme case is the NR with the highest Stokes shift, where no TE polarization was detected.

Our results shed light on many interesting phenomena of strong coupling between SPPs and different molecules. However, recent trends in polariton study are even more exciting. The modification of molecular energy levels in strong coupling regime was considered theoretically (31). It was shown that chemical reaction rates can be changed (44). Organic molecules are not two-level quantum emitters, but have complicated level structure, which include vibrational energy levels. In the case of strong coupling, energy is exchanged between the electromagnetic field and the molecule by the rate of Rabi frequency. This energy lays in between the nuclear and electronic energies and this can have effect on validity of Born-Oppenheimer approximation, which is at the heart of modern understanding of chemical reactions. Recently the strong coupling between an optical cavity mode and infrared vibrational transition in polymers was considered (57), (74). The Rabi splitting induces the shift of vibrational frequency and can have effect on chemical landscape of molecule namely by modification of the bond strength. The strong coupling employing SPPs in this frequency range has not been shown in case of metal structures.

Bibliography

[1] AGRANOVICH, V., LITINSKAIA, M., AND LIDZEY, D. G., *Cavity Polaritons in Microcavities Containing Disordered Organic Semiconductors*. Phys. Rev. B **67** (2003) 085311.

[2] AGRANOVICH, V. AND MILLS, D., *Surface Polaritons : Electromagnetic Waves at Surfaces and Interfaces* (1982).

[3] ARCHAMBAULT, A., MARQUIER, F., GREFFET, J.-J., AND ARNOLD, C., *Quantum Theory of Spontaneous and Stimulated Emission of Surface Plasmons*. Phys. Rev. B **82** (2010) 035411.

[4] ATWATER, H. A., DIONNE, J. A., AND LEZEC, H. J., *Negative refraction at visible frequencies*. Science **316** (2007) 430.

[5] BARNES, W., DEREUX, A., AND EBBESEN, T., *Surface Plasmon Subwavelength Optics*. Nature **424** (2003) 824.

[6] BARNES, W. L., *Topical review. Fluorescence near Interfaces: the Role of Photonic Mode Density.* Journal of Modern Optics **45** (1998) 661.

[7] BELLESSA, J., BONNAND, C., PLENET, J., AND MUGNIER, J., *Strong Coupling between Surface Plasmons and Excitons in an Organic Semiconductor*. Phys. Rev. Lett. **93** (2004) 036404.

[8] BILLSTEN, H., SUNDSTRÖM, V., AND POLÍVKA, T., *Self-Assembled Aggregates of the Carotenoid Zeaxanthin: Time-Resolved Study of Excited States*. J. Phys. Chem. A **109** (2005) 1521.

[9] BOLTASSEVA, A., NIKOLAJSEN, T., LEOSSON, K., KJAER, K., LARSEN, M., AND BOZHEVOLNYI, S., *Integrated Optical Components Utilizing Long-Range Surface Plasmon Polaritons*. Journal of Lightwave Technology **23** (2005) 413.

[10] BRAUNDMEIER, A. J. AND HALL, D. G., *Polarization Studies of Radiation Emitted by Surface Plasmons in Silver*. Optics Commun. **4** (1973) 343.

[11] BRAUNDMEIER, A. J. AND HALL, D. G., *Angular Dependence of Roughness-assisted Surface Plasmon Radiation: Comparison of Theory and Experiment*. Phys. Rev. B **17** (1975) 1557.

[12] BRAUNDMEIER, A. J. AND HALL, D. G., *Some Measurements of the Angular Distribution and Polarization of Surface Plasmon Radiation from Ag Films*. Surface Science **49** (1975) 376.

[13] BRAUNDMEIER, A. J. AND HALL, D. G., *Surface-Plasmon Radiation from Au and Ag Thin Films: The Surface Autocorrelation Function*. Phys. Rev. B **27** (1983) 624.

[14] BRENNECKE, C. F., *Collective Interaction Between a Bose-Einstein Condensate and a Coherent Few-Photon Field*. PhD thesis (2009).

[15] CASTANIÉ, A., *Surface Plasmon Hybridization in The Strong Coupling Regime in Gain Structures*. PhD thesis (2013).

[16] CHANCE, R., PROCK, A., AND SILBEY, R., *Molecular Fluorescence and Energy Transfer near Interfaces.* Adv. Chem. Phys. **37** (1978) 1.

[17] CHANG, R. AND CAMPILLO, A., *Optical processes in microcavities* (World Scientific, 1996).

[18] CHEN, H., SCHATZ, G. C., AND RATNER, M. A., *Experimental and Theoretical Studies of Plasmon-Molecule Interaction.* Rep. Prog. Phys. **75** (2012) 096402.

[19] COELLO, V., GARCIA-ORTIZ, C., AND GARCIA-MENDEZ, M., *Classical Plasmonics: Wave Propagation Control at Subwavelength Scale*. NANO: Brief Reports and Reviews **10** (2015) 1530005.

[20] COLES, D., GRANT, R., LIDZEY, D. G., CLARK, C., AND LAGOUDAKIS, P., *Imaging the Polariton Relaxation Bottleneck in Strongly Coupled Organic Semiconductor Microcavities*. Phys. Rev. B **88** (2013) 121303.

[21] COLES, D., P., M., CLARK, P. C., TSOI, W., ADAWI, A. M., KIM, J., AND LIDZEY, D., *Vibrationally Assisted Polariton-Relaxation Processes in Strongly Coupled Organic-Semiconductor Microcavities*. Adv. Funct. Mater. **21** (2011) 3691.

[22] COLES, D., SOMASCHI, N., MICHETTI, P., CLARK, C., LAGOUDAKIS, P., SAVVIDIS, P., AND LIDZEY, D., *Polariton-Mediated Energy Transfer between Organic Dyes in a Strongly Coupled Optical Microcavity*. Nature materials **13** (2014) 712.

[23] CORN, R. AND PHILPOTT, M., *Surface Plasmon Enhanced Raman Scattering at Thin Silver Films*. J. Chem. Phys **80** (1984) 5245.

[24] DINTINGER, J., KLEIN, S., BUSTOS, F., BARNES, W., AND EBBESEN, T., *Strong Coupling between Surface Plasmon-Polaritons and Organic Molecules in Subwavelength Hole Arrays*. Phys. Rev. B **71** (2005) 035424.

[25] DITLBACHER, H., KRENN, J. R., FELIGJ, N., LAMPRECHT, B., SCHIDER, G., SALERNO, M., LEITNER, A., AND AUSSENEGG, F. R., *Fluorescence Imaging of Surface Plasmon Fields.* Appl. Phys. Lett. **80** (2002) 404.

[26] DITLBACHER, H., KRENN, J. R., SCHIDER, G., LEITNER, A., AND AUSSENEGG, F. R., *Two-Dimensional Optics with Surface Plasmon Polaritons*. Appl. Phys. Lett. **81** (2002) 1762.

[27] EBBESEN, T. W., LEZEC, H., GHAEMI, H., THIO, T., AND WOLFF, P., *Extraordinary Optical Transmission through Sub-wavelength Hole Arrays*. Nature **391** (1998) 667.

[28] ENOCH, S. AND BONOD, N., *Plasmonics. From Basics to Advanced topics* (Springer, 2012).

[29] FEIST, J. AND GARCIA-VIDAL, F., *Extraordinary Exciton Conductance Induced by Strong Coupling*. Phys. Rev. Lett. **114** (2015) 196402.

[30] FISHER, T., AFSHAR, A., SKOLNICK, M., WHITTAKER, D., ROBERTS, J., HILL, G., AND PATE, M., *Electro-Optic Tuning of Vacuum Rabi Coupling in Semiconductor Quantum Microcavity Structures*. Solid State Electron. **40** (1996) 493.

[31] GALEGO, J., GARCIA-VIDAL, F. J., AND FEIST, J., *Cavity-Induced Modifications of Molecular Structure in the Strong Coupling Regime*. arXiv:1506.03331 (2015).

[32] GEDDES, C. D. AND LAKOWICZ, J. R., *Metal-Enhanced Fluorescence*. J. Fluoresc. **12** (2002) 121.

[33] GENTILE, M. J., HORSLEY, S. A. R., AND BARNES, W. L., *Localized ExcitonâPolariton Modes in Dye-Doped Nanospheres: a Quantum Approach*. arXiv:1506.01321 (2015).

[34] GEORGE, J., WANG, S., CHERVY, T., CANAGUIER-DURAND, A., SCHAEFFER, G., LEHN, J.-M., HUTCHISON, J., GENET, C., AND EBBESEN, T., *Ultra-Strong Coupling of Molecular Materials: Spectroscopy and Dynamics*. Faraday Discuss. **178** (2015) 281.

[35] GRYCZYNSKI, I., MALICKA, J., GRYCZYNSKI, Z., AND LAKOWICZ, J., *Radiative Decay Engineering 4. Experimental Studies of Surface Plasmon-coupled Directional Emission*. Anal. Biochem. **324** (2004) 170.

[36] GUEBROU, S. A., SYMONDS, C., HOMEYER, E., PLENET, J. C., GARTSTEIN, Y. N., AGRANOVICH, V. M., AND BELLESSA, J., *Coherent Emission from a Disordered Organic Semiconductor Induced by Strong Coupling with Surface Plasmons*. Phys. Rev. Lett. **108** (2012) 066401.

[37] HAKALA, T., TOPPARI, J., KUZYK, A., PETTERSSON, M., TIKKANEN, H., KUNTTU, H., AND TÖRMÄ, P., *Vacuum Rabi Splitting and Strong-Coupling Dynamics for Surface-Plasmon Polaritons and Rhodamine 6G Molecules*. Phys. Rev. Lett. **103** (2009) 053602.

[38] HAKALA, T., TOPPARI, J., PETTERSSON, M., TIKKANEN, H., KUNTTU, H., AND TÖRMÄ, P., *Frequency Conversion of Propagating Surface Plasmon Polaritons by Organic Molecules*. App. Phys. Lett. **93** (2008) 123307.

[39] HARBECKE, B., *The Coherent and Incoherent Reflection and Transmission of Multilayer Structures*. Appl. Phys. B **39** (1986) 165.

[40] HO, Z., HANSON, R., AND LIN, S. H., *Experimental and Theoretical Studies of Resonance Raman Scattering: Temperature Effects in β-carotene*. J. Chem. Phys. **77** (1982) 3414.

[41] HOMOLA, J., YEE, S., AND GAUGLITZ, G., *Surface Plasmon Resonance Sensors: Review*. Sensors and Actuators B **54** (1999) 3.

[42] HOUDRÉ, R., STANLEY, R., OESTERLE, U., ILEGEMS, M., AND WEISBUCH, C., *Room-Temperature Cavity Polaritons in a Semiconductor Microcavity*. Phys. Rev. B **49** (1994) 16761.

[43] HOUDRÉ, R., STANLEY, R., OESTERLE, U., PELLANDINI, P., AND ILEGEMS, M., *Measurement of Cavity-Polariton Dispersion Curve from Angle-Resolved Photoluminescence Experiments*. Phys. Rev. Lett. **73** (1994) 2043.

[44] HUTCHISON, J. A., SCHWARTZ, T., GENET, C., DEVAUX, E., AND EBBESEN, T. W., *Modifying Chemical Landscapes by Coupling to Vacuum Fields*. Angew. Chem. **124** (2012) 1624.

[45] IWASE, H., ENGLUND, D., AND VUČKOVIĆ, J., *Analysis of the Purcell Effect in Photonic and Plasmonic Crystals with Losses*. Optics Express **18** (2010) 16546.

[46] JOHNSON, P. AND CHRISTY, R., *Optical Constants of Nobel Metals*. Phys. Rev.B **6** (1972) 4370.

[47] KHURGIN, J., *How to Deal with the Loss in Plasmonics and Metamaterials.* Nature Nanotech. **10** (2015) 2.

[48] KIMBLE, H., *Strong Interactions of Single Atoms and Photons in Cavity QED.* Physica Scripta. **76** (1998) 127.

[49] KITSON, S. C., BARNES, W. L., AND SAMBLES, J. R., *A Full Photonic Band Gap for Surface Modes in the Visible.* Phys. Rev. Lett. **77** (1996) 2670.

[50] KOPONEN, M. A., HOHENESTER, U., HAKALA, T. K., AND TOPPARI, J. J., *Absence of Mutual Polariton Scattering for Strongly Coupled Surface Plasmon Polaritons and Dye Molecules with a Large Stokes Shift.* Phys. Rev. B **88** (2013) 085425.

[51] KRETSCHMANN, E., *The Angular Dependence and the Polarization of Light Emitted by Surface Plasmons on Metals Due to Roughness*. Optics Commun. **5** (1972) 331.

[52] LIDZEY, D., BRADLEY, D., SKOLNICK, M., VIRGILI, T., WALKER, S., AND WHITTAKER, D., *Strong Exciton-Photon Coupling in an Organic Semiconductor Microcavity*. Nature **395** (1998) 53.

[53] LIDZEY, D., FOX, A., RAH, M., SKOLNICK, M., AGRANOVICH, V., AND WALKER, S., *Experimental Study of Light Emission from Strongly Coupled Organic Semiconductor Microcavities following Nonresonant Laser Excitation*. Phys. Rev. B **65** (2002) 195312.

[54] LIDZEY, D., VIRGILI, T., BRADLEY, D., SKOLNICK, M., WALKER, S., AND WHITTAKER, D., *Observation of Strong Exciton-photon Coupling in Semiconductor Microcavities Containing Organic Dyes and J-Aggregates*. Optical Materials **12** (1999) 243.

[55] LIU, H., WANG, B., LEONG, E. P. S., YANG, P., ZONG, Y., SI, G., TENG, J., AND A., M. S., *Enhanced Surface Plasmon Resonance on a Smooth Silver Film with a Seed Growth Layer*. ASC Nano **4** (2010) 3139.

[56] LIU, Z., STEELE, J. M., SRITURAVANICH, W., PIKUS, Y., ZONG, Y., SUN, C., AND ZHANG, X., *Focusing Surface Plasmons with a Plasmonic Lens*. Nano Lett. **5** (2005) 1726.

[57] LONG, J. P. AND SIMPKINS, B. S., *Coherent Coupling between a Molecular Vibration and FabryâPerot Optical Cavity to Give Hybridized States in the Strong Coupling Limit*. ACS Photonics **2** (2015) 130.

[58] MAIER, S. A., *Plasmonics: Fundamentals and Applications* (Springer, 2007).

[59] MAIER, S. A., FRIEDMAN, M. D., BARCLAY, P. E., AND PAINTER, O., *Experimental Demonstration of Fiber-Accessible Metal Nanoparticle Plasmon Waveguides for Planar Energy Guiding and Sensing*. Appl. Phys. Lett. **86** (2005) 071103.

[60] MEYSTRE, P. AND SARGENT, M., *Elements of Quantum Optics* (Springer, 2007).

[61] MORELAND, J., ADAMS, A., AND HANSMA, P. C., *Efficiency of Light Emission from Surface Plasmons*. Phys. Rev. B **25** (1982) 2297.

[62] NIKOLAJSEN, T., LEOSSON, K., AND BOZHEVOLNYI, S., *Surface Plasmon Polariton Based Modulators and Switches Operating at Telecom Wavelengths*. Appl. Phys. Lett. **85** (2004) 5833.

[63] NIKOLAJSEN, T., LEOSSON, K., AND BOZHEVOLNYI, S., *In-Line Extinction Modulator Based on Long-Range Surface Plasmon Polaritons*. Optics Commun. **244** (2005) 455.

[64] NOGINOV, M., ZHU, G., BELGRAVE, A., BAKKER, R., SHALAEV, V., NARIMANOV, E., STOUT, S., HERZ, E., SUTEEWONG, T., AND WIESNER, U., *Demonstration of a Spaser-Based Nanolaser*. Nature **460** (2009) 1110.

[65] NOVOTNY, L., *Strong Coupling, Energy Splitting, and Level Crossings: A Classical Perspective*. Am. J. Phys. **78 (11)** (2010) 1199.

[66] NOVOTNY, L. AND HECHT, B., *Principles of Nano-Optics* (Cambridge University Press, 2006).

[67] ORGIU, E., GEORGE, J., HUTCHISON, J., DEVAUX, E., DAYEN, J., DOUDIN, B., STELLACCI, F., GENET, C., SCHACHENMAYER, J., GENES, C., PUPILLO, G., SAMORÍ, P., AND EBBESEN, T., *Conductivity in Organic Semiconductors Hybridized with the Vacuum Field*. J. Chern. Phys. **77** (1982) 6289.

[68] POCKRAND, I., BRILLANTE, A., AND MÖBIUS, D., *Exciton-Surface Plasmon Coupling: An Experimental Investigation*. J. Chern. Phys. **77** (1982) 6289.

[69] POLÍVKA, T. AND SUNDSTRÖM, V., *Ultrafast Dynamics of Carotenoid Excited States-From Solution to Natural and Artificial Systems*. Chem. Rev. **104** (2004) 2021.

[70] RAETHER, H., *Surface Plasmons On Smooth and Rough Surfaces and on Grattings* (Springer-Verlag, 1988).

[71] SALERNO, M., KRENN, J., LAMPRECHT, B., SCHIDER, G., DITLBACHER, H., FÃLIDJ, N., LEITNER, A., AND AUSSENEGG, F. R., *Plasmon Polariton in Metal Nanostructures: the Optoelectronic Route to Nanotechnology*. Opto-electronics Rev. **10** (2002) 217.

[72] SAVONA, V., ANDREANI, L., SCHWENDIMANN, P., AND QUATTROPANI, A., *Quantum Well Excitons in Semiconductor Microcavities: Unified Treatment of Weak and Strong Coupling Regimes*. Solid State Commun. **93** (1995) 733.

[73] SCHULLER, J. A., BARNARD, E. S., CAI, W., JUN, Y. C., WHITE, J. S., AND BRONGERSMA, M. L., *Plasmonics for Extreme Light Concentration and Manipulation*. Nature Materials **9** (2010) 193.

[74] SHALABNEY, A., GEORGE, J., HUTCHISON, J., PUPILLO, G., GENET, C., AND EBBESEN, T. W., *Coherent Coupling of Molecular Resonators with a Microcavity Mode*. Nat. Commun. **6** (2015) 5981.

[75] SHALAEV, V. AND KATAWA, S., *Nanophotonics with Surface Plasmons* (Elseviar, 2007).

[76] SKOLNICK, M., FISHER, T., AND WHITTAKER, D., *Topical review. Strong Coupling Phenomena in Quantum Microcavity Structures*. Semicond. Sci. Technol. **13** (1998) 645.

[77] STEINBERGER, B., HOHENAU, A., DITLBACHER, H., AUSSENEGG, F. R., LEITNER, A., AND KRENN, J. R., *Dielectric Stripes on Gold as Surface Plasmon Waveguides: Bends and Directional Couplers*. Appl. Phys. Lett. **91** (2007) 081111.

[78] STILES, P. L., DIERINGER, J., SHAH, N. C., AND VAN DUYNE, R. P., *Surface-Enhanced Raman Spectroscopy*. Annu. Rev. Anal. Chem. **1** (2008) 601.

[79] SYMONDS, C., BONNAND, C., PLENET, J. C., BRÃ©HIER, A., PARASHKOV, R., LAURET, J. C., DELEPORTE, E., AND BELLESSA, J., *Particularities of Surface PlasmonâExciton Strong Coupling with Large Rabi Splitting*. New Journal of Physics **10** (2008) 065017.

[80] TÖRMÄ, P. AND BARNES, W., *Strong Coupling between Surface Plasmon Polaritons and Emitters: a Review*. Rep. Prog. Phys. **78(1)** (2015) 016501.

[81] USHIODA, S. AND SASAKI, Y., *Raman Scattering Mediated by Surface-Plasmon Polariton Resonance*. Phys. Rev. B **27(2)** (1982) 1401.

[82] VAHALA, K., *Optical Microcavities.* Nature **424** (2003) 839.

[83] VALMORRA, F., BRÃ¶LL, M., SCHWAIGER, S., WELZEL, N., HEITMANN, D., AND MENDACH, S., *Strong Coupling between Surface Plasmon Polariton and Laser Dye Rhodamine 800.* App. Phys. Lett. **99** (2011) 051110.

[84] WEISBUCH, C., NISHIOKA, M., ISHIKAWA, A., AND ARAKAWA, Y., *Observation of the Coupled Exciton-Photon Mode Splitting in a Semiconductor Quantum Microcavity.* Phys. Rev. Lett. **69** (1992) 3314.

[85] WIEDERRECHT, G., HALL, J., AND BOUHELIER, A., *Control of Molecular Energy Redistribution Pathways via Surface Plasmon Gating*. Phys. Rev. Lett. **98** (2007) 083001.

[86] ZAYATS, A., SMOLYANINOV, I., AND MARADUDIN, A., *Nano-optics of Surface Plasmon Polaritons*. Phys. Rep. **408** (2005) 131.

[87] ZSILA, F., BIKÁDI, Z., DELIB, J., AND SIMONYIA, M., *Configuration of a Single Centre Determines Chirality of Supramolecular Carotenoid Self-Assembly.* Tetrahedron. Lett. **42** (2001) 2561.